



RIMBAY – a multi-approximation 3D ice-dynamics model for comprehensive applications: model description and examples

M. Thoma^{1,2}, K. Grosfeld¹, D. Barbi¹, J. Determann¹, S. Goeller¹, C. Mayer², and F. Pattyn³

¹Alfred Wegener Institute Helmholtz Center for Polar and Marine Research, Bussestrasse 24, 27570 Bremerhaven, Germany

²Bavarian Academy of Sciences, Commission for Glaciology, Alfons-Goppel-Str. 11, 80539 Munich, Germany

³Laboratoire de Glaciologie, Département des Sciences de la Terre et de l'Environnement (DSTE), Université Libre de Bruxelles (ULB), CP 160/03, Avenue F.D. Roosevelt, 1050 Bruxelles, Belgium

Correspondence to: M. Thoma (malte.thoma@awi.de)

Received: 30 May 2013 – Published in Geosci. Model Dev. Discuss.: 19 June 2013

Revised: 28 November 2013 – Accepted: 1 December 2013 – Published: 7 January 2014

Abstract. Glaciers and ice caps exhibit currently the largest cryospheric contributions to sea level rise. Modelling the dynamics and mass balance of the major ice sheets is therefore an important issue to investigate the current state and the future response of the cryosphere in response to changing environmental conditions, namely global warming. This requires a powerful, easy-to-use, versatile multi-approximation ice dynamics model. Based on the well-known and established ice sheet model of Pattyn (2003) we develop the modular multi-approximation thermomechanic ice model RIMBAY, in which we improve the original version in several aspects like a shallow ice–shallow shelf coupler and a full 3D-grounding-line migration scheme based on Schoof's (2007) heuristic analytical approach. We summarise the full Stokes equations and several approximations implemented within this model and we describe the different numerical discretisations. The results are cross-validated against previous publications dealing with ice modelling, and some additional artificial set-ups demonstrate the robustness of the different solvers and their internal coupling. RIMBAY is designed for an easy adaption to new scientific issues. Hence, we demonstrate in very different set-ups the applicability and functionality of RIMBAY in Earth system science in general and ice modelling in particular.

1 Introduction

According to the Fourth Assessment Report (AR4) of the Intergovernmental Panel on Climate Change (IPCC) (IPCC, 2007) it is unequivocal, that Earth's climate is warming since about 1850. This trend has been observed e.g. in rising air and ocean temperatures, in increased snow and ice melting, and in a rising sea level. According to more recent publications (e.g. Church et al., 2011; Rahmstorf et al., 2012) the trends estimated even for the worst scenarios of the AR4 are already reached or surpassed. Therefore, the imminent climate change will have profound impact on society (e.g. Hanson et al., 2011).

However, none of the complex numerical Earth system models (ESMs) in the IPCC report, used to compute the future climate trends, include the possible climate feedbacks of the large ice sheets in Greenland and Antarctica, resulting in large uncertainties for the global mean sea-level predictions.

These ice sheets play a crucial role in the Earth's hydrological cycle as they store about 75 % of the Earth's fresh water. In general, ice sheets accumulate mass from snow precipitation, which is compacted and finally transformed into ice. It follows the gravitational force and flows downhill from summits towards the ice sheet margin. However, this simplified view gets much more complex as different flow regimes exist within ice sheets (Fig. 1): the ice sheet's homogeneity is disturbed by nunataks and fast flowing ice streams; at the base, subglacial lakes and a hydrological network alternates the basal boundary conditions of the ice sheet; and at the edges ice shelves interact with the ocean by massive melting and

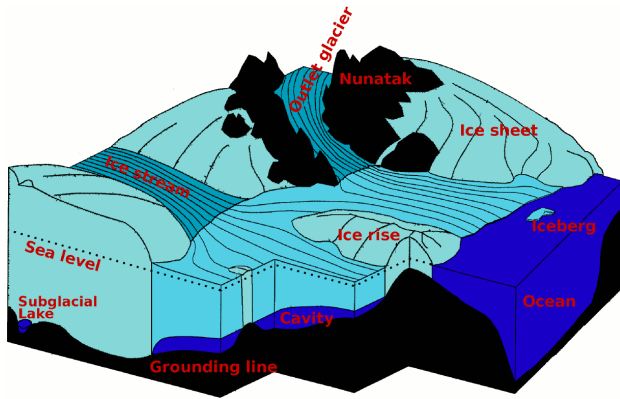


Fig. 1. Sketch illustrating several aspects/components to be considered in ice sheet modelling (adapted after Sandhäger, 2000).

iceberg calving. Therefore, a numerical model has to deal with many different aspects of an ice sheet (and ice shelf) to represent its complex dynamic behaviour adequately and to improve future projections or hindcasts for palaeoclimatology.

During the last years great efforts have been undertaken to improve existing ice models and to incorporate them into coupled climate models (e.g. Rutt et al., 2009; Gillet-Chaulet et al., 2012; Levermann et al., 2012). Here, we present the Revised Ice Model Based on frAnk pattYn, the multi-approximation ice sheet/ice shelf model RIMBAY. This model is originally based on the higher-order numerical ice-flow model of Pattyn (2003), which has been tested and applied to many scenarios (e.g. Pattyn, 2002; Pattyn et al., 2004; Pattyn, 2008, 2010). RIMBAY itself has been developed since 2009. Although the underlying higher order model (HOM) and full Stokes (FS)-physics remained basically unchanged, a shallow shelf approximation (SSA) solver has been added to calculate the horizontally averaged velocities of ice streams and ice shelves. Additionally, the numerical solver implementation, the discretisation, the coupling between different solvers and the user interface have been improved in many aspects since it diverted from the original model. Keeping in mind that ice models have to deal with many different geophysical settings and boundary conditions, it is challenging to design a computer code which is able to fulfil these needs for a large variety of users and applications. RIMBAY has been designed to be easy applicable to new scenarios, easy to extend and with clear interfaces to couple it with existing codes.

This paper is structured as follows: first, we clarify in Sect. 2 the sometimes imprecise usage of the term *model*, before we present in Sect. 3 the mathematical equations and several approximations founding the mathematical background of RIMBAY. Thereafter, we describe the numerical finite-difference implementation of these equations and how they can be solved with existing numerical solvers for linear

differential equations in Sect. 4. Some more details about the code implementation are given in Sect. 5, before we present some idealised example applications of RIMBAY, with a main focus on cross-validation with previously published ice-model results and an example of internal code coupling in Sect. 6. Finally, we demonstrate in Sect. 7 the wide spectrum of applications RIMBAY is already used for by several users.

2 Multi-approximation ice sheet/shelf model RIMBAY

The term *model* is used in several ways in Earth system science, which can be sometimes confusing. Therefore, we first define what we understand as *model* and, to be more precise, between which types of *models* we distinguish.

- Equations form the *mathematical model* describing the fundamental relationship between the relevant values of interest (e.g. velocity, temperature, and viscosity). In our context, these equations are mostly coupled differential equations which can not be solved analytically.
- These equations are solved with a computer, which requires a discretisation of the equations. This can be done in several distinct ways, depending on the demand of accuracy, stability, convergence properties, and resources (memory usage and computational cost). We refer to this as the *numerical model*.
- This numerical model has to be translated into a computer language (mostly a high-level programming language like Matlab, Fortran, C, or C++). It is common sense to refer to this computer program as *model*, too. We use the expression *code* or the *implementation* to specify the lines forming this (sometimes compiled binary) program.
- Finally, the code is applied to answer a specific scientific question (e.g. the contribution to sea level rise) of a specific domain (e.g. whole Antarctica or a subregion like the area of the Pine Island Glacier), or to study processes (e.g. the impact of basal water on ice dynamics) and the sensitivity to parameters or boundary conditions (e.g. geothermal heat flux, bedrock topography or ice thickness distribution). These applications of a computer program are often called *model*, too. We refer to these applications as *experiments* or *scenarios*.

In general, we use the term RIMBAY for the implementation of the discretised equation, and therefore the compiled binary code, which includes not only the mathematical model, but also a sophisticated command-line interpreter and input-output interfaces for an easy usage. RIMBAY is distributed with a suit of example – and reference – scenarios and several

additional programs (mainly based on the bash-script language) providing several options to visualise the computed results with the generic mapping tools (GMT) (GMT, Wessel and Smith, 1998; Wessel et al., 2013). In the following sections, we elaborate on these different model types and how they are used in RIMBAY.

3 Mathematical model

The mathematical field equations are based upon the conservation of mass, momentum, and energy:

$$\frac{\partial \rho}{\partial t} + \nabla \cdot (\rho \mathbf{v}) = 0, \quad (1)$$

$$\rho \frac{d\mathbf{v}}{dt} = \nabla \cdot \boldsymbol{\tau} + \rho \mathbf{g}, \quad (2)$$

$$\rho c \frac{d\theta}{dt} = \nabla \cdot (\kappa \nabla \theta) + Q_i, \quad (3)$$

with the (constant) density ρ , the velocity vector $\mathbf{v} = (v_x, v_y, v_z) = (u, v, w)$, the gravitational acceleration $\mathbf{g} = (0, 0, -g)$, the two dimensional stress tensor $\boldsymbol{\tau}$, the (potential) temperature θ , the heat capacity c , the thermal conductivity κ , and the internal frictional heating Q_i . In the following we consider Cartesian coordinates, with the vertical coordinate z upwards and neglect acceleration. In case of an incompressible fluid with a constant density the continuity equation (conservation of mass) follows as

$$\nabla \cdot \mathbf{v} = \frac{\partial u}{\partial x} + \frac{\partial v}{\partial y} + \frac{\partial w}{\partial z} = 0. \quad (4)$$

The stress tensor $\boldsymbol{\tau}$ is split into a deviatoric part $\boldsymbol{\tau}'$ and an isotropic pressure, which is defined as the negative trace of the stress tensor:

$$\begin{aligned} \boldsymbol{\tau} &= \boldsymbol{\tau}' + \frac{1}{3} (\tau_{xx} + \tau_{yy} + \tau_{zz}) \mathbf{1} \\ &= \boldsymbol{\tau}' - p \mathbf{1}, \end{aligned} \quad (5)$$

where $\mathbf{1}$ symbolises the identity matrix.

3.1 Equation of motion

Because velocities in ice sheet/shelf modelling are rather small, acceleration can be ignored and the momentum equation can be written as

$$\begin{aligned} \frac{\partial \tau'_{xx}}{\partial x} + \frac{\partial \tau'_{xy}}{\partial y} + \frac{\partial \tau'_{xz}}{\partial z} - \frac{\partial p}{\partial x} &= 0, \\ \frac{\partial \tau'_{yx}}{\partial x} + \frac{\partial \tau'_{yy}}{\partial y} + \frac{\partial \tau'_{yz}}{\partial z} - \frac{\partial p}{\partial y} &= 0, \\ \frac{\partial \tau'_{zx}}{\partial x} + \frac{\partial \tau'_{zy}}{\partial y} + \frac{\partial \tau'_{zz}}{\partial z} - \frac{\partial p}{\partial z} &= \rho g. \end{aligned} \quad (6)$$

According to Paterson (1994), the constitutive equation for polycrystalline ice links the deviatoric stresses to the strain rates,

$$\begin{aligned} \boldsymbol{\tau}' &= 2\eta \dot{\boldsymbol{\epsilon}} = 2\eta \begin{pmatrix} \dot{\epsilon}_{xx} & \dot{\epsilon}_{xy} & \dot{\epsilon}_{xz} \\ \dot{\epsilon}_{yx} & \dot{\epsilon}_{yy} & \dot{\epsilon}_{yz} \\ \dot{\epsilon}_{zx} & \dot{\epsilon}_{zy} & \dot{\epsilon}_{zz} \end{pmatrix} \\ &= 2\eta \begin{pmatrix} \frac{\partial u}{\partial x} & \frac{1}{2} \left(\frac{\partial u}{\partial y} + \frac{\partial v}{\partial x} \right) & \frac{1}{2} \left(\frac{\partial u}{\partial z} + \frac{\partial w}{\partial x} \right) \\ \frac{1}{2} \left(\frac{\partial u}{\partial y} + \frac{\partial v}{\partial x} \right) & \frac{\partial v}{\partial y} & \frac{1}{2} \left(\frac{\partial v}{\partial z} + \frac{\partial w}{\partial y} \right) \\ \frac{1}{2} \left(\frac{\partial u}{\partial z} + \frac{\partial w}{\partial x} \right) & \frac{1}{2} \left(\frac{\partial v}{\partial z} + \frac{\partial w}{\partial y} \right) & \frac{\partial w}{\partial z} \end{pmatrix}, \end{aligned} \quad (7)$$

applying the effective viscosity η , which can be described by the Glen-type flow law (e.g. Cuffey and Paterson, 2010):

$$\begin{aligned} \dot{\boldsymbol{\epsilon}} &= A(\hat{\theta}) \boldsymbol{\tau}'^n, \quad \text{or} \quad \boldsymbol{\tau}' = 2\eta \dot{\boldsymbol{\epsilon}} \quad \text{with} \\ \eta &:= \frac{1}{2} A(\hat{\theta})^{-\frac{1}{n}} \dot{\boldsymbol{\epsilon}}^{\frac{(1-n)}{n}}, \end{aligned} \quad (8)$$

with $n = 3$, the pressure-corrected ice temperature $\hat{\theta} = \theta + \alpha p$, with a constant $\alpha = 9.8 \times 10^{-4} \text{ K Pa}^{-1}$ (Greve and Blatter, 2009), and the effective strain rate (valid for incompressibility as $\dot{\epsilon}_{xx} + \dot{\epsilon}_{yy} + \dot{\epsilon}_{zz} = 0$ follows from Eq. 4)

$$\dot{\boldsymbol{\epsilon}} = \sqrt{\dot{\epsilon}_{xx}^2 + \dot{\epsilon}_{yy}^2 + \dot{\epsilon}_{zz}^2 + \dot{\epsilon}_{xx}\dot{\epsilon}_{yy} + \dot{\epsilon}_{xy}^2 + \dot{\epsilon}_{xz}^2 + \dot{\epsilon}_{yz}^2}. \quad (9)$$

The temperature dependent *rate factor* $A(\hat{\theta})$ is parameterised according to the Arrhenius relationship after Hooke (1981) or Paterson and Budd (1982). Combining Eq. (6) and Eq. (7) we get the so-called full Stokes (FS) equations for ice modelling:

$$\begin{aligned} \frac{\partial}{\partial x} \left(2\eta \frac{\partial u}{\partial x} \right) + \frac{\partial}{\partial y} \left(\eta \frac{\partial u}{\partial y} + \eta \frac{\partial v}{\partial x} \right) \\ + \frac{\partial}{\partial z} \left(\eta \frac{\partial u}{\partial z} + \eta \frac{\partial w}{\partial x} \right) - \frac{\partial p}{\partial x} &= 0, \\ \frac{\partial}{\partial x} \left(\eta \frac{\partial u}{\partial y} + \eta \frac{\partial v}{\partial x} \right) + \frac{\partial}{\partial y} \left(2\eta \frac{\partial v}{\partial y} \right) \\ + \frac{\partial}{\partial z} \left(\eta \frac{\partial v}{\partial z} + \eta \frac{\partial w}{\partial y} \right) - \frac{\partial p}{\partial y} &= 0, \\ \frac{\partial}{\partial x} \left(\eta \frac{\partial u}{\partial z} + \eta \frac{\partial w}{\partial x} \right) + \frac{\partial}{\partial y} \left(\eta \frac{\partial v}{\partial z} + \eta \frac{\partial w}{\partial y} \right) \\ + \frac{\partial}{\partial z} \left(2\eta \frac{\partial w}{\partial z} \right) - \frac{\partial p}{\partial z} &= \rho g. \end{aligned} \quad (10)$$

Rearranging Eq. (5) leads to

$$\begin{aligned} p &= -\tau'_{xx} - \tau'_{yy} - \tau_{zz} \\ &= -2\eta \left(\frac{\partial u}{\partial x} + \frac{\partial v}{\partial y} \right) - \tau_{zz}, \end{aligned} \quad (11)$$

with an expression for the vertical normal stress τ_{zz} obtained by vertically integrating the third equation of Eq. (6) from the

surface S to the height z (Van der Veen and Whillans, 1989; Pattyn, 2008):

$$\tau_{zz} = -\rho g(S - z) + \underbrace{\frac{\partial}{\partial x} \int_z^S \tau'_{xz} dz' + \frac{\partial}{\partial y} \int_z^S \tau'_{yz} dz'}_{R_{zz}}. \quad (12)$$

Here, the first term in Eq. (12) describes the hydrostatic part and R_{zz} the resistive part, sometimes also referred to as *vertical resistive longitudinal stress*.

Depending on the scientific issue, several approximations of Eq. (10) might be reasonable, which are described in the following subsection.

3.2 Higher-order approximation

The HOM approximation of Pattyn (2003) applies the hydrostatic approximation, by neglecting the resistive stress R_{zz} in Eqs. (10)–(12) for the vertical velocity and the vertical normal stress. These are only relevant (but still almost two orders of magnitude below the other normal stress and shear stress components, Pattyn, 2000) where the ice flow regime changes, as in the vicinity of ice margins or ice divides. Additionally, ignoring the horizontal derivatives of the vertical velocity in Eq. (10), leads to

$$\begin{aligned} \frac{\partial}{\partial x} \left(2\eta \frac{\partial u}{\partial x} \right) + \frac{\partial}{\partial y} \left(\eta \frac{\partial u}{\partial y} + \eta \frac{\partial v}{\partial x} \right) \\ + \frac{\partial}{\partial z} \left(\eta \frac{\partial u}{\partial z} \right) - \frac{\partial p}{\partial x} = 0, \\ \frac{\partial}{\partial x} \left(\eta \frac{\partial u}{\partial y} + \eta \frac{\partial v}{\partial x} \right) + \frac{\partial}{\partial y} \left(2\eta \frac{\partial v}{\partial y} \right) \\ + \frac{\partial}{\partial z} \left(\eta \frac{\partial v}{\partial z} \right) - \frac{\partial p}{\partial y} = 0, \\ \frac{\partial}{\partial z} \left(2\eta \frac{\partial w}{\partial z} \right) - \frac{\partial p}{\partial z} = \rho g. \end{aligned} \quad (13)$$

Applying Eqs. (11) and (12) we obtain

$$\begin{aligned} \frac{\partial}{\partial x} \left[2\eta \left(2 \frac{\partial u}{\partial x} + \frac{\partial v}{\partial y} \right) \right] + \frac{\partial}{\partial y} \left[\eta \left(\frac{\partial u}{\partial y} + \frac{\partial v}{\partial x} \right) \right] \\ + \frac{\partial}{\partial z} \left(\eta \frac{\partial u}{\partial z} \right) = \rho g \frac{\partial S}{\partial x}, \\ \frac{\partial}{\partial y} \left[2\eta \left(2 \frac{\partial v}{\partial y} + \frac{\partial u}{\partial x} \right) \right] + \frac{\partial}{\partial x} \left[\eta \left(\frac{\partial u}{\partial y} + \frac{\partial v}{\partial x} \right) \right] \\ + \frac{\partial}{\partial z} \left(\eta \frac{\partial v}{\partial z} \right) = \rho g \frac{\partial S}{\partial y}, \end{aligned} \quad (14)$$

for the horizontal velocities. The vertical velocity at depth z can be derived by integrating the continuity equation Eq. (4) from the base B vertically:

$$w(z) = w(B) - \int_B^z \left(\frac{\partial u}{\partial x} + \frac{\partial v}{\partial y} \right) dz'. \quad (15)$$

3.3 Shallow shelf or shelfy stream approximation

A second common approximation is the shallow shelf approximation or shelfy stream approximation (SSA). This assumes that the horizontal velocity is depth-independent ($\frac{\partial u}{\partial z} = \frac{\partial v}{\partial z} = 0$), which is the case for ice shelf regions and fast flowing ice streams decoupled from the ground. Integrating Eq. (14) through the ice from the base B to the surface S , and defining U and V as the vertically integrated velocities leads to (e.g. Morland, 1987; MacAyeal, 1989; Pattyn, 2010)

$$\begin{aligned} \frac{\partial}{\partial x} \left[2H\eta \left(2 \frac{\partial U}{\partial x} + \frac{\partial V}{\partial y} \right) \right] + \frac{\partial}{\partial y} \left[H\eta \left(\frac{\partial U}{\partial y} + \frac{\partial V}{\partial x} \right) \right] \\ - \tau_{bx} = \rho g H \frac{\partial S}{\partial x}, \\ \frac{\partial}{\partial y} \left[2H\eta \left(2 \frac{\partial V}{\partial y} + \frac{\partial U}{\partial x} \right) \right] + \frac{\partial}{\partial x} \left[H\eta \left(\frac{\partial U}{\partial y} + \frac{\partial V}{\partial x} \right) \right] \\ - \tau_{by} = \rho g H \frac{\partial S}{\partial y}, \end{aligned} \quad (16)$$

where the basal shear stress τ_{bi} retards the otherwise unhampered flow on bedrock till. It can be expressed in terms of the basal friction parameter β^2 and the horizontal velocity: $\tau_{bi} = \beta^2 V_i$. A thorough derivation of Eq. 16 can be found in Greve and Blatter (2009). Both, the shelfy stream approximation and the shallow shelf approximation are expressed by Eq. (16). The only difference is, that for an ice shelf or above a subglacial lake β^2 is zero, while it might reach several thousand Pa a m⁻¹ for a slippery bedrock, which especially applies to basal lubricated areas. As a rule of thumb above dry bedrock a value of $\beta^2 = 25\,000$ Pa a m⁻¹ would correspond to a typical frictional stress of about 100 kPa (Paterson, 1994) if a velocity of about 4 m a⁻¹ is assumed (Thoma et al., 2012). Finally, because of the lacking vertical shear stresses Eq. (9) reduces to

$$\dot{\epsilon} = \sqrt{\dot{\epsilon}_{xx}^2 + \dot{\epsilon}_{yy}^2 + \dot{\epsilon}_{xx}\dot{\epsilon}_{yy} + \dot{\epsilon}_{xy}^2}. \quad (17)$$

3.4 Shallow ice approximation

The most rigid approximation is the shallow ice approximation (SIA, which is a reasonable simplification for large ice bodies, when the horizontal length scale is much larger than the ice thickness (e.g. Hutter, 1983). Assuming that the horizontal derivation of the vertical velocity is much smaller than the vertical derivation of the horizontal velocity ($\frac{\partial w}{\partial x} \ll \frac{\partial u}{\partial z}$) and applying the hydrostatic approximation (which reduces the vertical momentum balance to the hydrostatic term) we derive

$$\begin{aligned} \frac{\partial}{\partial z} \left(\eta \frac{\partial u}{\partial z} \right) - \frac{\partial p}{\partial x} = 0, \\ \frac{\partial}{\partial z} \left(\eta \frac{\partial v}{\partial z} \right) - \frac{\partial p}{\partial y} = 0, \\ - \frac{\partial p}{\partial z} = \rho g. \end{aligned} \quad (18)$$

Basically, this approximation decouples the horizontal velocities, allowing local solutions for the velocity field, instead of a much more complex and time-consuming implicit solver. The numerical resources of this SIA are so low (compared to any other approximations) that it is still widely used (and useful) for many applications.

3.5 Boundary conditions

Several boundary conditions have to be formulated to solve the different approximations of the equation of motion.

1. We apply a stress-free *surface* boundary condition:

$$\boldsymbol{\tau}_s \cdot \mathbf{n}_s = 0, \quad (19)$$

with the normal vector \mathbf{n}_s orthogonal to the surface.

2. For the horizontal velocities at the ice *base*, we apply either

- a no-slip condition for the tangential velocities ($\mathbf{v}_{\parallel} = \mathbf{v}_b - \mathbf{n}_b(\mathbf{v}_b \cdot \mathbf{n}_b) = 0$).
- a Weertman-type sliding law (e.g. Paterson, 1994; Cuffey and Paterson, 2010), linking the sliding velocity with the basal shear stress:

$$\begin{aligned} \boldsymbol{\tau}_b &= \beta^2 \mathbf{v}_b &= C |\mathbf{v}_b|^{m-1} \mathbf{v}_b & \text{or} \\ \mathbf{v}_b &= \frac{1}{\beta^2} \boldsymbol{\tau}_b &= C^{-\frac{1}{m}} |\boldsymbol{\tau}_b|^{\frac{1}{m}-1} \boldsymbol{\tau}_b, \end{aligned} \quad (20)$$

with the basal tangential stress component $\boldsymbol{\tau}_b = \boldsymbol{\tau} \cdot \mathbf{n}_b$ and the normal vector \mathbf{n}_b orthogonal to the ice base, the basal friction coefficient C , and the basal friction exponent m .

The basal drag is defined as the sum of all basal resistive forces (Van der Veen and Whillans, 1989; Pattyn, 2003):

$$\begin{aligned} \tau_{bx} &= \tau'_{xz} - \left(2\tau'_{xx} + \tau'_{yy} + R_{zz} \right) \frac{\partial B}{\partial x} - \tau'_{xy} \frac{\partial B}{\partial y} \\ \tau_{by} &= \tau'_{yz} - \left(2\tau'_{yy} + \tau'_{xx} + R_{zz} \right) \frac{\partial B}{\partial y} - \tau'_{xy} \frac{\partial B}{\partial x} \end{aligned} \quad (21)$$

with $\tau'_{ij} = \tau'_{ij}(B)$. In case of the SIA these equations simplify to

$$\tau_{bx} = -\rho g H \frac{\partial S}{\partial x}, \quad \tau_{by} = -\rho g H \frac{\partial S}{\partial y}. \quad (22)$$

- or a stress free base when a substantial amount of water is present, like in the case of subglacial lakes and ice shelves; this implies $\beta^2 = 0$.

3. For the vertical velocity at the base, we apply a kinematic boundary condition:

$$w_B = \frac{\partial B}{\partial t} + u \frac{\partial B}{\partial x} + v \frac{\partial B}{\partial y} - \dot{m}_B, \quad (23)$$

with the basal melt rate \dot{m}_B .

4. At *lateral boundaries* of the model domain, we apply either

- zero ice thickness ($H = 0$),
- Dirichlet boundary conditions with fixed velocities. The no-slip condition ($u = 0$), which would imply frozen ice at nunataks, is a special case of this.
- A Neumann free-slip boundary condition:
$$\nabla v_i \cdot \mathbf{n}_i = 0,$$

$$[\nabla(\mathbf{v} - (\mathbf{v} \cdot \mathbf{n}_{\perp})\mathbf{n}_{\perp})] \mathbf{n}_{\perp} = 0, \quad (24)$$

at ice-nunatak edges, with the unit vector \mathbf{n}_{\perp} orthogonal to the edge, or

- a (dynamic) Neumann boundary condition for an ice shelf–ocean interface (e.g. Greve and Blatter, 2009; Joughin et al., 2009; Pattyn, 2010),

$$\begin{aligned} 2\mu H \left(2 \frac{\partial U}{\partial x} + \frac{\partial V}{\partial y} \right) n_x \\ + \mu H \left(\frac{\partial U}{\partial y} + \frac{\partial V}{\partial x} \right) n_y &= \frac{\rho g H S n_x}{2}, \\ 2\mu H \left(2 \frac{\partial V}{\partial y} + \frac{\partial U}{\partial x} \right) n_y \\ + \mu H \left(\frac{\partial V}{\partial x} + \frac{\partial U}{\partial y} \right) n_x &= \frac{\rho g H S n_y}{2}, \end{aligned} \quad (25)$$

with the outward-pointing unit vector (n_x, n_y) , which is perpendicular to the (vertical) ice shelf front.

- or periodic boundary conditions.

These equations are converted in terrain following σ coordinates by applying

$$\sigma = \frac{S - z}{H}, \quad (26)$$

with the ice thickness H and the surface height S . This coordinate transformation leads to additional metric terms in the equations, which are described in detail in Pattyn (2003) or Greve and Blatter (2009). The advantage is, that the vertical coordinate ranges from $\sigma = 0$ at the surface to $\sigma = 1$ at the ice base, independent of the local ice thickness and the bedrock elevation.

3.6 Temperature calculation

Assuming a constant thermal conductivity κ , the temperature evolution (Eq. 3) can be divided into an advective, a diffusive and a source term:

$$\rho c \left(\frac{\partial \theta}{\partial t} + \underbrace{\mathbf{v} \cdot \nabla \theta}_{\text{Advection}} \right) = \underbrace{\kappa \nabla^2 \theta}_{\text{Diffusion}} + \underbrace{Q_i}_{\text{Internal Sources}}. \quad (27)$$

Neglecting horizontal diffusion and assuming that the internal heat source results mainly from the ice deformation (Paterson, 1994) we obtain with the effective deviatoric stress τ' (defined similar to the effective strain rate in Eq. 9) and $Q_i = 2\dot{\epsilon}\tau' = 4\eta\dot{\epsilon}^2$

$$\frac{\partial\theta}{\partial t} = \frac{\kappa}{\rho c} \frac{\partial^2\theta}{\partial z^2} - u \frac{\partial\theta}{\partial x} - v \frac{\partial\theta}{\partial y} - w \frac{\partial\theta}{\partial z} + \frac{4\eta\dot{\epsilon}^2}{\rho c}. \quad (28)$$

The boundary conditions applied to solve this thermodynamic equation are

- the mean air temperature at the surface of the ice body,
- a Dirichlet boundary condition according to the pressure melting point of ice (e.g. Paterson, 1994), $\theta = -8.7 \times 10^{-4} \text{ K m}^{-1} H$, at the ice base when the ice is floating (like above subglacial lakes and for ice shelves), and
- a Neumann boundary condition at the base b for grounded ice:

$$\frac{\partial\theta_b}{\partial z} = -\frac{G + \tau'_b |\mathbf{v}_b|}{\kappa}, \quad (29)$$

with the basal stress $\tau'_b = \sqrt{\tau_{bx}^2 + \tau_{by}^2}$ and the geothermal heat flux G .

3.7 Ice sheet evolution

Integration of Eq. (1) from the base B to the surface S leads to an equation for the ice evolution. Defining the ice thickness $H = S - B$, accounting for melting or accumulation at the surface and/or base and assuming a constant ice density ρ we get

$$\frac{\partial}{\partial t} \int_B^S \rho dz + \nabla \cdot \int_B^S (\rho \mathbf{v}_i) dz = \rho \dot{m}, \quad (30)$$

$$\frac{\partial H}{\partial t} = - \left(\frac{\partial UH}{\partial x} + \frac{\partial VH}{\partial y} \right) + \dot{m}, \quad (31)$$

with the mass balance (in m a^{-1}) is defined as

$$\dot{m} = \underbrace{\dot{m}_{ac}}_{\text{Accumulation}} - \underbrace{\dot{m}_{ab}}_{\text{Ablation}} - \underbrace{\dot{m}_B}_{\text{Basal melting}}. \quad (32)$$

Basal freezing can be implemented by negative basal melting.

4 Numerical model

4.1 Linear and non-linear solvers

The coupled pair of equations for the horizontal velocity field for the FS, HOM, and SSA equations (Eqs. 10, 14, 16)

depend on the strain-rate dependent viscosity (Eq. 8), resulting in a non-linear problem. In the full Stokes case, the horizontal velocities depend also on the vertical velocity. However, these problems can be solved iteratively as indicated in Fig. 2.

In the full Stokes case, the vertical velocity w can be estimated from the continuity Eq. (4), imposing kinematic boundary condition at the lower ice surface (including melt rates).

According to Pattyn (2003), it is sufficient to solve the system of linear equations for u and v successively, instead of solving both equations at once. In general, we iteratively solve

$$A_{nm}(x_{ij}^l) \cdot x_m^{l+1} = b_n(x_{ij}^l), \quad (33)$$

where l is the iteration, A_{nm} contains the coefficients of the left-hand side of the relevant equation to solve, while b_n is the forcing term on the right-hand side of the equation. The placeholder x_m symbolises the horizontal velocities u_{ij} or v_{ij} (Eqs. 10, 14, or 16), the potential temperature θ_{ij} (Eq. 28), or the ice thickness H_{ij} (Eq. 31), respectively. The indices n and m symbolise the consecutively numbered grid nodes from $(j = 1, i = 1)$ to $(j = X_{\max}, i = Y_{\max})^1$.

Two methods to solve the linear system of Eq. (33) are available within RIMBAY: first, the fast and efficient biconjugate gradient method with a Jacobian preconditioner (*linbcg*) from the numerical recipes (NR) (Press et al., 2007); second, the Library of Iterative Solvers (LIS) from Nishida (2010).

The Library of Iterative Solvers (LIS) provides a bunch of preconditioners and solvers, including the recommendable generalised minimal residual (gmres) method, which can also be applied to solve non-symmetric matrices. For both methods the effective *compressed row storage* (CRS) sparse matrix method is used as a default to store the elements of the matrix A_{nm} . However, for the LIS, the *modified sparse row* (MSR) format is implemented, too. Comparisons with respect to the calculated velocities have shown

- the differences for the two storage formats (CRS vs. MSR) are negligible,
- the differences between the *linbcg* solver from Press et al. (2007) and the very same preconditioner/solver combination from the Library of Iterative Solvers are negligible, but the solver of Press et al. (2007) needs less computational resources.
- if specific preconditioner–solver combinations converge, the difference between different combinations are negligible.

Summarised, if a solution of the linear system can be computed with a reasonable accuracy, the results can be trusted.

¹Note, that for historical reasons (originating from Pattyn, 2003, 2008) the order of i and j is swapped within RIMBAY, compared with the intuitive usage.

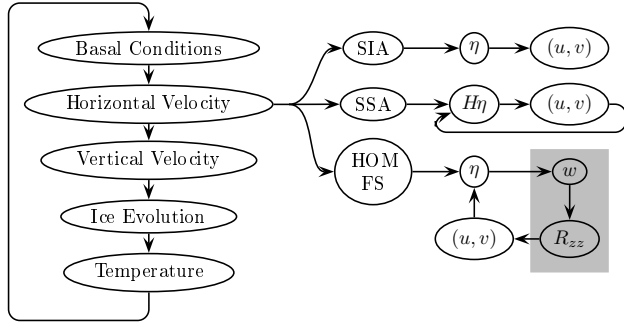


Fig. 2. Sequence of iteratively solved variables within RIMBAY. In the SSA case the product of $H\eta$ is calculated, instead of the viscosity η , only. The grayish highlighted variables are calculated only in the FS case. (Within the main loop, the vertical velocity needs only to be calculated in the non-FS cases.)

In general, we suggest to start with the faster linbcg algorithm (from Press et al., 2007) and to switch to the gmres solver with a Jacobian or ILU (Incomplete LU decomposition) preconditioner if it should fail.

When solving the linearised equations for the horizontal velocity, the viscosity η might vary over a few orders of magnitude, which requires a sophisticated convergence scheme. Hence, a simple Picard iteration might fail. Therefore, Pattyn (2003) extended this scheme by the unstable manifold correction (UMC), introduced by Hindmarsh and Payne (1996), which results in a proper convergence of the solution. In RIMBAY the UMC is applied in the SSA, HOM, and FS solvers.

4.2 Discretisation

When equations are discretised, it is important to realise where exactly the individual variables are located. This is quite simply defined for the unstaggered Arakawa A-grid (e.g. Arakawa and Lamb, 1977; Purser and Leslie, 1988) where all variables are located in the very same grid position. However, sometimes a different approach has numerical advantages. Besides the traditional (unstaggered) A-grid, the staggered Arakawa C-grid is optionally available in RIMBAY for the SIA and SSA solvers. On the Arakawa C-grid, the horizontal velocities are defined in between the thickness (and viscosity) nodes as illustrated in Fig. 3.

4.3 Ice Sheet evolution

As an example, we formulate the implemented discretisation of the ice sheet evolution (Eq. 31) explicitly for the two different grids. Additionally, the detailed discretisation on the C-grid of the SSA equation of motion (Eq. 16) is given in Appendix B.

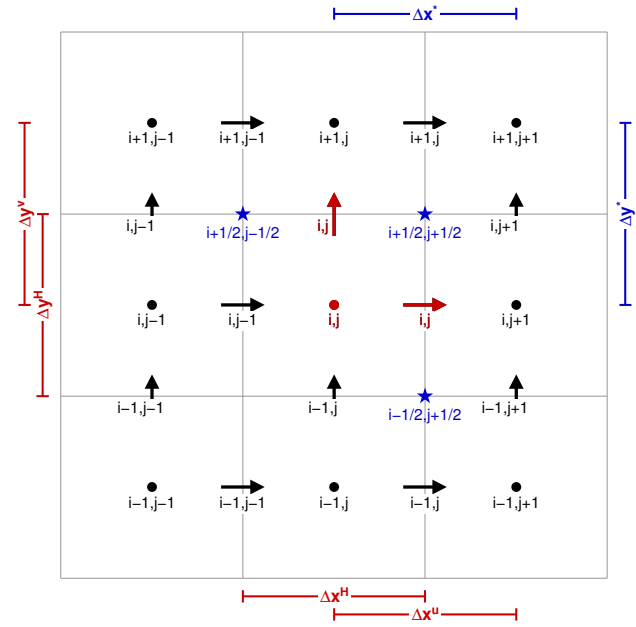


Fig. 3. Location of nodes on a C-grid. The location of H , η , and θ nodes are indicated by dots while the location of the horizontal velocities are indicated by arrows. The stars indicate certain inter-grid nodes used in the numerical implementation. The red colour indicates corresponding nodes of the central i, j node and the colour-coded increments ($\Delta \dots$) at the edges refer to the corresponding grid node distances.

4.3.1 C-grid

For the C-grid, where the velocities are defined in-between thickness nodes, the equation of the ice sheet evolution (Eq. 31) can be written as an implicit first order finite difference equation as

$$\begin{aligned}
 H_{i,j}^{t+1} &+ \frac{\Delta t \left[U_{i,j} (H_{i,j+1}^{t+1} + H_{i,j}^{t+1}) - U_{i,j-1} (H_{i,j}^{t+1} + H_{i,j-1}^{t+1}) \right]}{2\Delta x} \\
 &+ \frac{\Delta t \left[V_{i,j} (H_{i+1,j}^{t+1} + H_{i,j}^{t+1}) - V_{i-1,j} (H_{i,j}^{t+1} + H_{i-1,j}^{t+1}) \right]}{2\Delta y} \\
 &= H_{i,j}^t + \dot{m} \Delta t.
 \end{aligned} \tag{34}$$

Rearranging Eq. (34) with respect to the five discrete H^{t+1} values, located and numbered as indicated in Fig. 4, results in the following coefficients for the sparse matrix A_{nm} of the linear solver:

$$\begin{aligned}
 C_{n1} &= -\frac{\Delta t}{2\Delta y} V_{i-1,j}, \\
 C_{n2} &= -\frac{\Delta t}{2\Delta x} U_{i,j-1}, \\
 C_{n3} &= 1 + \frac{\Delta t}{2} \left(\frac{U_{i,j} - U_{i,j-1}}{\Delta x} + \frac{V_{i,j} - V_{i-1,j}}{\Delta y} \right),
 \end{aligned}$$

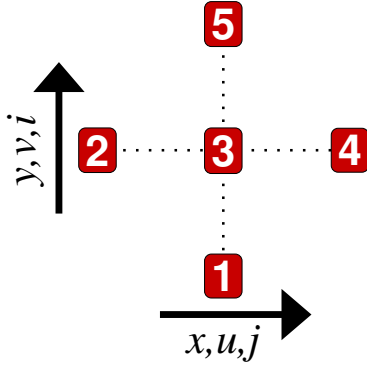


Fig. 4. Relative positions and numbering of nodes for the implicit first order finite difference formulation of the ice evolution (Eq. 31).

$$\begin{aligned}
 C_{n4} &= + \frac{\Delta t}{2\Delta x} U_{i,j}, \\
 C_{n5} &= + \frac{\Delta t}{2\Delta y} V_{i,j}, \\
 b_n &= H_{i,j}^t + \dot{m}_{i,j} \Delta t.
 \end{aligned} \quad (35)$$

These coefficients represent the non-zero elements of each single row n for each i, j element of the matrix A_{nm} , with C_{n3} indicating the central node at (i, j) and b_n the forcing term on the right-hand side.

The coefficients derived in the last subsection are valid for the interior of the ice. Boundary conditions have to be formulated at the edges of the ice sheet. *Open boundaries* for grid cells adjacent to ocean or ice-free land are simply implicitly implemented by assuming $H = 0$ at the respective grid cell.

If the ice adjoins a nunatak or a lateral end of the model domain, *closed boundary* conditions are applied. We define these by setting the velocity (and thus the flux) of ice over the edge of the specific grid cell, to zero. For example, closed boundaries at the eastern ($U_{i,j} = 0$) and southern ($V_{i-1,j} = 0$) edges would result in $C_{n1} = C_{n4} = 0$ and $C_{n3} = 1 + \frac{\Delta t}{2} \left(\frac{V_{i,j}}{\Delta y} - \frac{U_{i,j-1}}{\Delta x} \right)$ in Eq. (35).

4.3.2 A-grid

For the the A-grid a pure advective scheme to solve Eq. (31) would be numerically problematic, because of the velocity–pressure gradient coupling. Hence, we decompose the equation into a weighted advective and diffusive part by applying the identity $(\nabla H + \nabla B)(\nabla S)^{-1} = 1$, derived from a simple gradient formulation of $S = H + B$ (surface elevation S equals ice thickness H plus ice bottom B):

$$\begin{aligned}
 \frac{\partial H}{\partial t} + f_{ad} \nabla \cdot [V_i H (\nabla S)^{-1} (\nabla H + \nabla B)] \\
 + (1 - f_{ad}) \nabla \cdot (V_i H) = \dot{m},
 \end{aligned} \quad (36)$$

with $f_{ad} = 1$ for pure diffusion and $f_{ad} = 0$ in case of pure advection. With the definition of the non-linear (because

it depends on the solution H) diffusion vector $D_i := (D_x, D_y) = -V_i H (\nabla S)^{-1}$ we derive

$$\begin{aligned}
 \frac{\partial H}{\partial t} - f_{ad} \nabla \cdot (D_i \nabla H) + (1 - f_{ad}) \nabla \cdot (V_i H) \\
 = f_{ad} \nabla \cdot (D_i \nabla B) + \dot{m}.
 \end{aligned} \quad (37)$$

The finite difference formulation of Eq. (37) as well as the coefficients C_{nm} for the sparse linear matrix for the interior and the boundary conditions are given in the Appendix A. In general, it would be appropriate to apply the diffusive equation (with $f_{ad} = 1$), because a *Lax* method has to be used to numerically stabilise the advective part of Eq. (37) (see Appendix A). Unfortunately, this adds numerical dissipation (numerical diffusion) and results in a time-step dependence of the solution. However, if the ice body contains ice shelves and/or ice divides with flat areas, the reciprocal value of $(\nabla S)^{-1}$ becomes very large and counteracts the stabilising effect of the otherwise stable diffusive implementation. Despite this problem of exchanging stability towards convergence (with respect to decreasing time steps) this approach has been discussed in some applications (e.g. Pattyn et al., 2006; Docquier et al., 2011).

As an alternative to overcome the restrictions involved with the numerical representation with respect to $(\nabla S)^{-1}$ in Eq. (36), we implemented a mass conserving (time step independent) upwind scheme, based on Eq. (34). Averaging the horizontal velocities from their central (A-grid) location towards the grid-cell edges according to $U_{i,j}^c = \frac{1}{2}(U_{i,j} + U_{i,j+1})$ and $V_{i,j}^c = \frac{1}{2}(V_{i,j} + V_{i+1,j})$ leads to

$$\begin{aligned}
 H_{i,j}^{t+1} + \frac{\Delta t}{2\Delta x} \left[(U_{i,j}^c + |U_{i,j}^c|) H_{i,j}^{t+1} + (U_{i,j}^c - |U_{i,j}^c|) H_{i,j+1}^{t+1} \right. \\
 \left. - (U_{i,j-1}^c + |U_{i,j-1}^c|) H_{i,j-1}^{t+1} - (U_{i,j-1}^c - |U_{i,j-1}^c|) H_{i,j}^{t+1} \right] \\
 + \frac{\Delta t}{2\Delta y} \left[(V_{i,j}^c + |V_{i,j}^c|) H_{i,j}^{t+1} + (V_{i,j}^c - |V_{i,j}^c|) H_{i+1,j}^{t+1} \right. \\
 \left. - (V_{i-1,j}^c + |V_{i-1,j}^c|) H_{i-1,j}^{t+1} - (V_{i-1,j}^c - |V_{i-1,j}^c|) H_{i,j}^{t+1} \right] \\
 = H_{i,j}^t + \dot{m} \Delta t,
 \end{aligned} \quad (38)$$

and the following coefficients for the sparse matrix A_{nm} :

$$\begin{aligned}
 C_{n1} &= - \frac{\Delta t}{2\Delta y} (V_{i-1,j}^c + |V_{i-1,j}^c|), \\
 C_{n2} &= - \frac{\Delta t}{2\Delta x} (U_{i,j-1}^c + |U_{i,j-1}^c|), \\
 C_{n3} &= 1 + \frac{\Delta t}{2} \left(\frac{(U_{i,j}^c + |U_{i,j}^c|) - (U_{i,j-1}^c - |U_{i,j-1}^c|)}{\Delta x} \right. \\
 &\quad \left. + \frac{(V_{i,j}^c + |V_{i,j}^c|) - (V_{i-1,j}^c - |V_{i-1,j}^c|)}{\Delta y} \right),
 \end{aligned}$$

$$\begin{aligned}
C_{n4} &= + \frac{\Delta t}{2\Delta x} (U_{i,j}^c - |U_{i,j}^c|), \\
C_{n5} &= + \frac{\Delta t}{2\Delta y} (V_{i,j}^c - |V_{i,j}^c|), \\
b_n &= H_{i,j}^t + \dot{m}_{i,j} \Delta t.
\end{aligned} \tag{39}$$

4.4 Ice sheet–ice shelf coupling and grounding line flux

The mechanically correct way of coupling a ice sheet system with an ice shelf system would be a FS approach. According to Pattyn et al. (2013) a horizontal resolution of less than 0.5 km is necessary to capture the grounding line (GRL) migration accurately. This however, is computationally costly and inefficient, especially for major parts of the ice sheet and ice shelf, which are at a large distance from the GRL where reduced physics is sufficient (see Eqs. 16 and 18, respectively). Either a finite element discretisation (as in the Elmer/ice model or the Ice Sheet System Model (ISSM), e.g. Zwinger et al., 2007; Larour et al., 2012) or a finite volume approach are necessary to implement FS physics in a reasonable way. Another approach to increase the grid resolution in specific regions of interest are adaptive grids (e.g. Gladstone et al., 2010; Cornford et al., 2013), although they have (to our knowledge) not been applied to HOM or FS physics, yet. For coarse resolution finite difference models (with grid sizes beyond one kilometre), Pollard and DeConto (2009) and Pollard and DeConto (2012) suggested a heuristic approach, based on the semi-analytical grounding line flux solution, derived by Schoof (2007):

$$\begin{aligned}
Q_x^S &= \left(\frac{A(\rho g)^{n+1} (1 - \rho/\rho_{\text{Ocean}})^n}{4^n C} \right)^{\frac{1}{m+1}} \\
&\quad \left(\frac{\tau'_{xx}}{\tau_f} \right)^{\frac{n}{m+1}} h_g^{\frac{m+n+3}{m+1}},
\end{aligned} \tag{40}$$

with the longitudinal stress τ'_{xx} just downstream of the grounding line, and the unbuttressed stress $\tau_f = 0.5 \rho g h_g (1 - \rho/\rho_{\text{Ocean}})$. The grounding line flux Q_x^S is estimated from the ice thickness h_g at the interpolated sub-grid grounding line position. Before the ice evolution Eq. (30) is solved, the Schoof flux (estimated on a sub-grid scale) constrains the flux across the grounding line by correcting the previous estimated velocity, located on a discrete grid node according to

$$\begin{aligned}
u &= \frac{Q_x^S}{H} & v &= \frac{Q_y^S}{H} & \text{A-grid,} \\
u &= \frac{2Q_x^S}{H + H_{\text{float}}} & v &= \frac{2Q_y^S}{H + H_{\text{float}}} & \text{C-grid.}
\end{aligned} \tag{41}$$

With the ice thickness H at the last grounded node (the model's grounding line) and H_{float} the ice thickness at the first floating node downstream. The distinction depends on the relation between the analytical Schoof-flux Q_i^S and the

modelled flux through the last gridded node $Q_i^M = V_i H$ (or $Q_i^M = V_i \cdot 0.5(H + H_{\text{float}})$ on a C-grid): if $Q_i^S \geq Q_i^M$ then more ice is transported into the ice shelf and the grounding line retreats or stays constant, the velocity at the grounding line is corrected according to Eq. (41). If $Q_i^S < Q_i^M$ then less ice is transported into the ice shelf and more ice is kept in the ice sheet, the grounding line advances and the velocity of the first floating node is corrected according to Eq. (41). A detailed description of this method is given in Docquier et al. (2011), Pollard and DeConto (2012), and Pattyn et al. (2012). To avoid unrealistic velocity steps, we additionally apply a conservative 2D-Gaussian filter to the grounding line nodes to smooth the resulting velocity field.

5 Implementation

5.1 General Information

The RIMBAY code is mainly² written in C++ and has about 30 000 (mostly) well documented lines. For historical reasons the code is not completely object oriented yet, the majority is organised into classes, and the number of global variables (which should be avoided as much as possible in any code) is close to zero. A reasonable degree of code separation into several C++ classes, allows an easy maintenance of the code. Well-defined interfaces (public methods of the C++ classes) enable an easy extension of the code for upcoming developments in ice modelling and/or further reaching applications (see Sect. 7).

The *GNU build system*³ (also known as the *autotools*) is a suite of programming tools designed to assist in making source-code packages portable to many Unix-like systems. It generates system- and environment-dependent *Makefiles* automatically and attends dependencies between different source (and header) files. Thanks to the *GNU build system*, RIMBAY has been compiled and tested successfully on several different Unix-platforms without any code adjustments. To distribute, develop, and maintain RIMBAY we use the distributed revision control system *monotone*⁴, which keeps track of any changes within the code and provides a sophisticated automatic merging of development branches.

One of the main programming paradigms for RIMBAY is that the very same (compiled) code has to run every single (previous successfully tested) scenario without any code editing and/or recompiling. To achieve this, RIMBAY is started with command-line arguments and loads the specific scenario from parameter files and (if requested) optionally from a netcdf file, too. The well established netcdf output format of

²A few parts of RIMBAY are still based on the original code of Pattyn (2003, 2008), which was written in C and not C++; also the implemented solver libraries (from NR and LIS), and the netcdf interface are written in C.

³http://en.wikipedia.org/wiki/GNU_build_system.

⁴<http://www.monotone.ca/>.

RIMBAY ensures that the computed results can subsequently be post-processed with the desired software packages, if the supplied GMT-bash scripts (Wessel and Smith, 1998; Wessel et al., 2013) (included in the RIMBAY-monotone database) should not be sufficient.

The RIMBAY code comes with a test suite containing nearly 50 different scenarios. These small and fast-running scenarios are designed to ensure that future model developments do not interfere with previous results.

5.2 Solver coupling

The coupling of SIA and SSA at the grounding line is realised by applying depth averaged velocities from the SIA solver as a Dirichlet boundary condition for the SSA solver. This transition can be located either at the last grounded node (the numerical GRL) or several grid nodes inside the ice sheet. In the latter case a *transition zone* (or *grounding zone*) is defined by a region where the solutions of the SIA and the SSA solvers are interpolated.

If the HOM/FS should not be applied to the whole model domain (which might be reasonable to save computational time), one or more *region(s) of interest* can be defined. In that case, the resource-consuming HOM/FS solver is limited to these regions only, while the faster SIA and SSA solvers are applied elsewhere and provide the Dirichlet boundary conditions for the HOM/FS solver (see example in Sect. 6.4).

6 Validation

The implementation of the different mathematical models (SIA, SSA, HOM, and FS) to calculate the horizontal velocity field are validated separately in this subsection. Additionally we show that the solver for the ice sheet evolution and the solver coupling produces reasonable results. The temperature evolution and thermomechanical coupling is not reconsidered here. Although the solvers have been revised, their results are identical to those published by Pattyn (2003) and Thoma et al. (2012).

6.1 SIA solver

The A-grid implementation of the SIA within RIMBAY is mainly identical to those of Pattyn (2003) and has already been validated successfully against the *moving-margin Eismint* benchmark described in Huybrechts et al. (1996) within Pattyn (2003). Here, we compare the estimated ice thicknesses, derived with the A-grid (Type-II according to Huybrechts et al., 1996) and the C-grid RIMBAY implementation for the *fixed-* and *moving-margin* benchmark experiments, with results published by Huybrechts et al. (1996) and Bueller et al. (2005). Figure 5 shows that the A-grid implementation produces results very close to the reference, while the C-grid implementation results in a 0.38% larger ice thickness. Considering the very different discretisations (compare

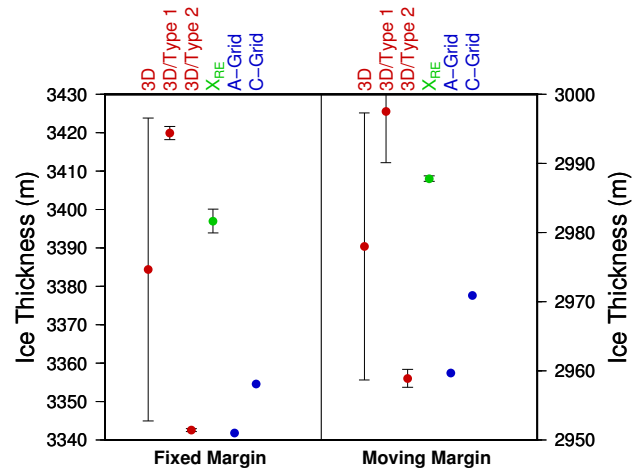


Fig. 5. Comparison of modelled SIA ice thicknesses of experiments described in Huybrechts et al. (1996) (red), the *Richardson extrapolation* result of Bueller et al. (2005) (green), and RIMBAY results (blue). The RIMBAY A-grid implementation corresponds essentially with the 3D/Type-II.

Eqs. 34 and A2) of the ice evolution equation, this is acceptable.

6.2 SSA solver

The A- and the C-grid implementations of the SSA are compared with a diagnostic tabular iceberg experiment of Jansen et al. (2005). In this experiment, the horizontal velocity field of a rectangular iceberg with a constant thickness of 250 m and an isothermal temperature of -2°C is calculated. The viscosity is calculated according to Eq. (8) with $n = 3$ and a temperature dependent rate factor given by the Arrhenius relationship after Paterson and Budd (1982). Our horizontal velocities are calculated on a 1 km grid and are in close agreement with those presented by Jansen et al. (2005) (Fig. 6a). Additionally, we rotate the iceberg, to demonstrate the independence of the model results from the iceberg's orientation within the rectangular grid (Fig. 6b–e). This test is essential for the modelling of evolving ice sheet fronts, which are rarely aligned with the grid orientation in real geometries.

A much more complex proof-of-concept is shown in Fig. 7. This artificially constructed geometry with a grid resolution of 2 km features

- a non-constant ice thickness;
- two discontinuous areas, which are solved simultaneously by the numerical solver;
- a quite complex shaped ice–water front with corners, tongues, and an inlet at $x \approx 200$ km.
- The brown areas in Fig. 7 symbolise nunataks, where special boundary conditions are applied: In the south

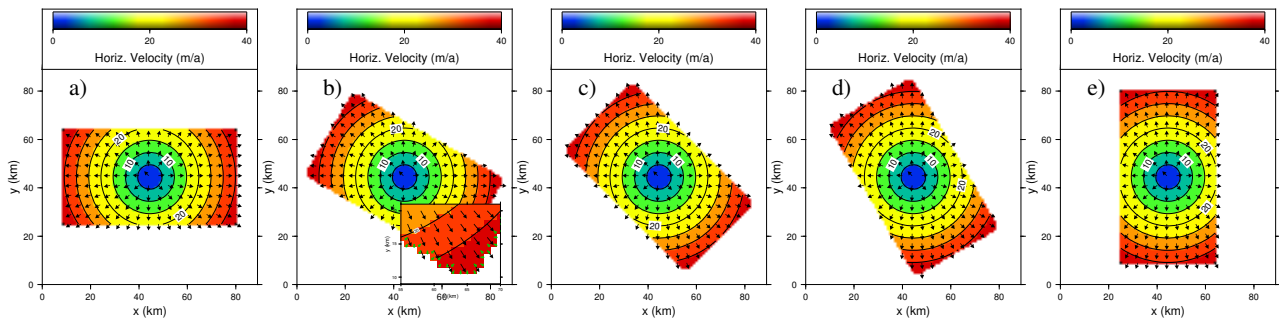


Fig. 6. Modelled horizontal velocity for a synthetic iceberg in different orientations. The enlarged inlet shows exemplarily the orientation of the normal vectors at the ice shelf front in green (compare Eq. 25).

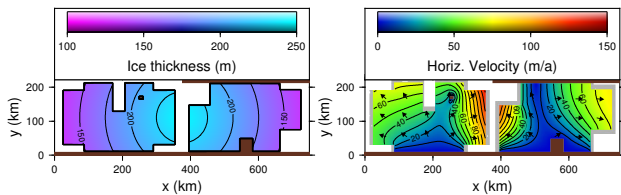


Fig. 7. Modelled horizontal velocity for two synthetic floating ice structures of complex geometries. Nunataks are indicated in brown. At the southern (lower) edge no-slip boundary conditions are applied, at the northern edge and at the ice rise in the left ice body free-slip boundaries are valid.

($y = 0$), a no-slip boundary results in stagnation at the ice–nunatak interface, while at the northern edge ($y = 220$ km) of the right iceberg a free-slip boundary condition is applied.

- Additionally, a small nunatak (with an area of $10 \text{ km} \times 5 \text{ km} = 50 \text{ km}^2$) located within the left iceberg with free-slip boundary conditions is added.

The modelled velocity pattern is consistent with the expectations, which are

- higher velocities at higher ice fronts,
- zero velocities at no-slip boundaries, and
- a reduced, orthogonally orientated velocity field at free-slip boundaries.

The difference between the A-grid and the C-grid (not shown) are negligible. Therefore, we conclude that the SSA-solver implementation produces reasonable and robust results, even for complex geometries.

6.3 SIA–SSA solver coupling and GRL migration

The results of the Marine Ice Sheet Model Intercomparison Project (MISMIP) (Pattyn et al., 2012) are a good benchmark test for the capability of a coupled ice sheet/shelf model

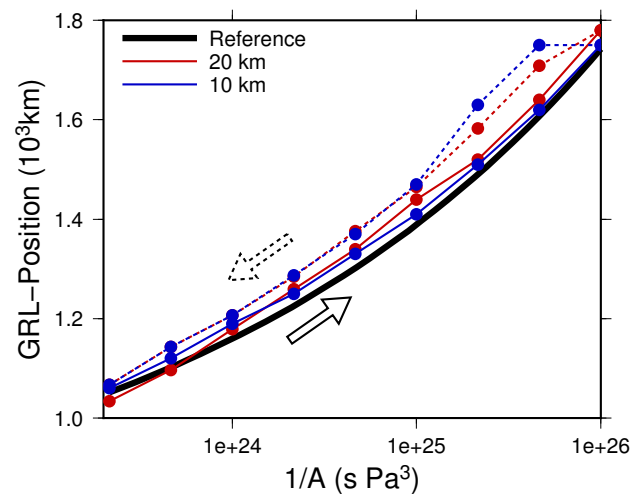


Fig. 8. Steady state grounding-line positions according to the boundary layer theory of Schoof (2007) (black) for a 2D-flow-line experiment Pattyn et al. (2012). Modelled RIMBAY GRL positions for different resolutions with advancing (solid) and retreating (dashed) GRL are indicated as a function of ice viscosity.

to predict grounding line migrations. In this 2D flow-line experiment the position of the GRL is compared with the boundary layer theory of Schoof (2007). We applied RIMBAY with different horizontal resolutions and a transition zone of 100 km, imposing the heuristic condition according to the method described in Sect. 4.4. Figure 8 indicates that the semi-analytical steady state grounding-line positions, according to the boundary layer theory of Schoof (2007), are in general reproduced well with RIMBAY. However, some delayed movements happen because of numerical issues in this idealised set-up.

Recently, RIMBAY participated in the extended 3D variant of the MISMIP, which investigates the grounding line response to external forcings (Pattyn et al., 2013). We performed different scenarios with comparable coarse resolutions between 2 and 20 km, because our main focus was on the applicability of these approximations with respect to

large-scale modelling, possibly coupled with an atmosphere and ocean model in an Earth system model approach. For reversibility tests and transient experiments only the 5 km and 10 km resolutions were considered. In order to overcome the problem of capturing grounding line migration in coarse resolutions, we apply the heuristic rule described in Sect. 4.4. Despite the rather coarse resolution (compared with most of the other 15 participating numerical ice models), RIMBAY accomplished the velocity-field comparison of the diagnostic experiment and in particular the reversibility test for grounding line migration. The latter is a prerequisite for modelling the Antarctic Ice Sheet, which is surrounded by ice shelves along more than half of its coast line. However, as a consequence of the imposed heuristic grounding line condition, which is not valid for a compressive flow, RIMBAY is (as all other A-HySSA models that participated in the MISIP3d intercomparison) incapable of reproducing a grounding line retreat at free-slip walls. Despite the partly discontinuous grounding line retreat, resulting from the rather coarse resolution, we conclude that RIMBAY is capable of simulating large ice bodies with attached ice shelves for different climate conditions.

6.4 HOM and FS solvers

The numerical core for the HOM solver is very similar to the original implementation of Pattyn (2003), validated in the the Ice Sheet Model Intercomparison Project for higher order models (ISMIP-HOM) experiments (Pattyn et al., 2008). The FS implementation is basically an extension of this code and has originally been published in Pattyn (2008) for a linear rheology (with $n = 1$ in Eq. 8) and successfully been expanded for non-linear rheologies (with $n = 3$) by Thoma et al. (2010, 2012). The results of these specific code-fragments are already published, hence we do not present any additional validation of the FS solution here.

However, we present two coupled SIA–FS–SSA experiments to demonstrate the flexibility of RIMBAY, with respect of a nested HOM/FS domain within a SIA–SSA domain.

The first experiment, is simply an extension of the original MISIP experiment discussed in Sect. 6.3 and Fig. 8. In addition to the coupled SIA–SSA solver, we modelled an area of 250 km in the vicinity of the GRL with the HOM and FS solver, respectively. We confined this test to the highest viscosity applied in Pattyn et al. (2012) ($1/A = 2.1544 \times 10^{23} \text{ s Pa}^3$), where the modelled grounding line position is at about 1058.7 km (Fig. 8). Applying the HOM solver in the vicinity of the grounding line, after the SIA–SSA model reached a steady state, results in a slight retreat of about 8 km (which is below the grid size of 10 km) to 1051.3 km. This result is in close agreement with the theoretical position (1051.9 km) according to the boundary layer theory of Schoof (2007). Switching from the HOM solver to the FS solver, however, does not change the GRL position anymore

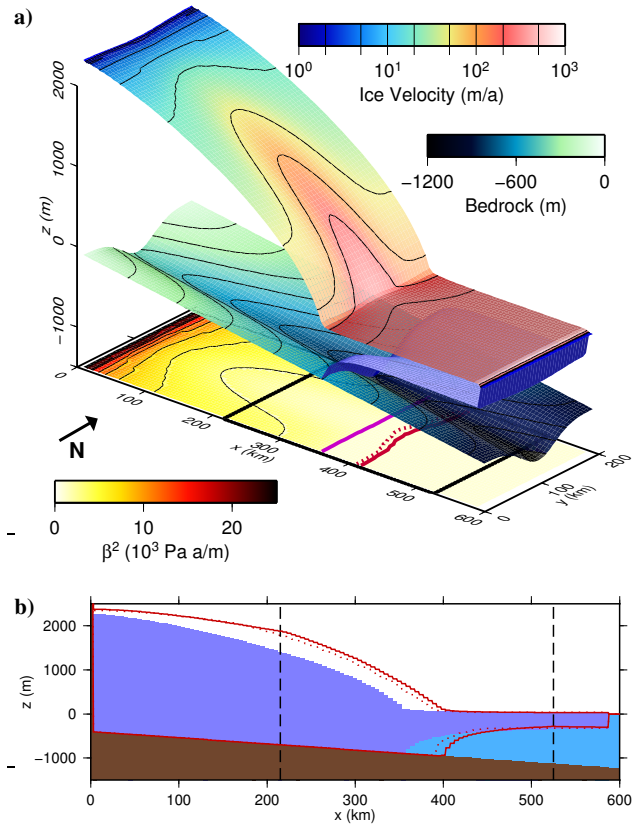


Fig. 9. Geometry for the experiment described in Sect. 6.4.

(a) Bedrock topography and ice geometry. The horizontal ice velocity is plotted on top of the ice sheet surface; the magenta and red lines indicate the interpolated (sub-grid scale) GRL-positions for the coupled SIA–SSA, the HOM (dotted) and the FS (solid) solutions, respectively; the black rectangle indicates the region, where the FS solver is applied. Additionally, the basal friction parameter β^2 (according to Eq. 20) is shown.

(b) Profile along $y = 100$ km. The dashed black lines indicate the area where the HOM and FS solutions are calculated, respectively; the red lines indicate the shape of the corresponding ice geometry for the HOM solution (dotted) and FS solution (solid).

significantly, neither does an extension of the HOM/FS domain from 250 km up to 900 km.

In the second experiment, the bedrock is downward sloping with a central trough:

$$B = -100 \text{ m} - 1.5x - 300 \cdot e^{-\left(\frac{y-100 \text{ km}}{40 \text{ km}}\right)^2}, \quad (42)$$

the horizontal resolution is 5 km and the accumulation is set to $\dot{m}_{ac} = 0.5 \text{ m a}^{-1}$ (Fig. 9a). A Weertman-type sliding law (Eq. 20) is applied as basal boundary condition, modified with an additional basal sliding reduction in the model's domain centre according to

$$C = C' \left[1 - 0.5 \exp \left(-\frac{(x-x_j)^2}{2x_i^2} - \frac{(y-y_j)^2}{2y_i^2} \right) \right], \quad (43)$$

with $C' = 10^7 \text{ Pa m}^{-1/3} \text{ s}^{1/3}$, $m = \frac{1}{3}$, $x_j = 300 \text{ km}$, $x_i = 100 \text{ km}$, $y_j = 100 \text{ km}$, and $y_i = 10 \text{ km}$ (this reduction is similar to those applied in Pattyn et al., 2013). The ice is surrounded by nunataks in the south, west, and north and an ocean in the east. We apply $dS/dx = 0$ at the western ice divide, free-slip boundary conditions along the southern and northern nunataks and the dynamic boundary conditions according to Eq. (25) at the ice–ocean boundary. First, the model is run with the coupled SIA–SSA solver and a transition zone of 50 km (imposing the heuristic condition outlined in Sect. 4.4 at the grounding line) until a steady state is reached. Within the transition zone, the SIA and the SSA solutions for the velocity field are interpolated. The final steady state of this control experiment is shown in Fig. 9a, indicating the ice’s geometry as well as the vertically averaged horizontal velocity.

Thereafter, (first) the HOM solver and (later) the FS solver are applied to the region, indicated in Fig. 9. As a result the grounding line advantages from 356 km to 398 km (HOM) and 408 km (FS solver), respectively, in this synthetic experiment. Pattyn et al. (2012, 2013) and Drouet et al. (2013) already discussed the limitations of the SIA–SSA approximations with respect to grounding line migration and pointed out that a high spatial resolution would be necessary to map the whole dynamic behaviour of transient states in ice sheet models.

However, in ice sheet/ice shelf models on a continental or even global scale and on long timescales (millennia), a high spatial resolution (below 10 km) and a FS solver, which consumes significant more computational resources than the SIA–SSA approximations, might be too ambitious at present. With respect to the large uncertainties of other atmospheric and ocean modelling issues, like boundary conditions and parameterisations, the drawback of the SIA–SSA approximation might be tolerable for most large-scale applications.

7 Conclusions

We have shown, that RIMBAY is capable of reproducing results of previously published experiments and benchmark tests (upper part of Table 1). In addition, RIMBAY has already been successfully applied in many very different scenarios in recent years. These applications range from high-resolution FS modelling of ice flow across subglacial lakes (Thoma et al., 2010, 2012) in studies concerning the interaction between ice sheet, ice shelf and the ocean with a coupled SIA–SSA solver (Determann et al., 2012, 2014; Pattyn et al., 2013), to coupling RIMBAY with the Community Earth System Models (COSMOS) (Barbi et al., 2013) and the Viscoelastic Lithosphere and Mantle model (VILMA) (Konrad et al., 2013, 2014), which calculates the isostatic adjustment of a spherical Earth to (ice-)surface loads.

Two additional modules are implemented within RIMBAY, broadening its versatility: first, the *water layer concept*,

developed by Goeller et al. (2013a), providing a sophisticated concept for the evolution of a large-scale subglacial hydrological network, which interacts with the ice sheet by modifying the basal boundary conditions. Second, a sub-grid scale Lagrangian-tracer module, allowing to track tracer propagation through the ice, which assists with the interpretation of the origin and age of ice cores (Sutter et al., 2013). All mentioned applications and modules are summarised in Table 1.

Several numerical ice flow model codes have been developed over the past years. In particular, the more recent FE approaches to solve the FS equations, as implemented in the ISSM (Larour et al., 2012; Seroussi et al., 2012) and ELMER/ICE (e.g. Zwinger et al., 2007; Gillet-Chaulet et al., 2012), are very promising. Their ability to adjust the spatial grid resolution with respect to the area under investigation is very useful. Their main drawbacks are currently the computational resources needed, which prohibit long-term projections on millennial timescales, and that (at least to the author’s knowledge) there is no general concept of moving grids, which could adjust along a migrating area of investigation. To our knowledge only ISSM has the potential of coupling models of varying orders of complexity (SIA/SSA/HOM/FS) (Seroussi et al., 2012).

Well-known FD thermomechanically coupled ice sheet models are the Community Ice Sheet Models (CISM, based on GLIMMER; Payne, 1999; Rutt et al., 2009; Bougamont et al., 2011; Lemieux et al., 2011), the Parallel Ice Sheet Model (PISM; Martin et al., 2011; Winkelmann et al., 2011), the PennState3D ice-sheet/shelf model (PenState3D; Pollard and DeConto, 2012) and the SIMulation COde for POLythermal Ice Sheets (SICOPOLIS; Greve, 1995; Sato and Greve, 2012). A recent overview about the most up-to-date ice sheet models is given by Bindschadler et al. (2013). All these models have proven their flexibility in several applications. However, none of these coupled SIA–SSA models has the option to simulate selected domains (e.g. the vicinity of grounding lines or ice streams) within a larger (e.g. continental scale) area with a (potentially migrating) FS approach.

With RIMBAY we provide a versatile open-source ice dynamics model to the scientific community. The code is not parallelised yet (apart from the LIS), and can be run even on common single-processor Linux or Unix systems. RIMBAY can be redistributed and/or modified under the terms of the GNU General Public License as published by the Free Software Foundation, either 3rd (or any later) version of the license⁵. RIMBAY fills a gap between several demands of the ice sheet modelling community, because it combines (a) the simplicity of a finite difference model, which can be run on a single processor, with (b) the option to model selected regions with a HOM or FS model, and (c) the potential to apply

⁵The GNU licence can be found at <http://www.gnu.org/licenses/gpl>. However, please be aware that the solver library LIS is released under the *BSD License* and that the code based on the Numerical Recipes (NR) is copyrighted.

Table 1. Validation and applications of the ice sheet/shelf model RIMBAY. The FS experiments appear as validation as well, as there is no explicit benchmark available. The two FS validations differ, as Thoma et al. (2010) extended the originally linear flow law used by Pattyn (2008).

Topic	Resolution (km)	Solver	Grid	Reference
<i>Validation</i>				
Eismint	50	SIA	A&C	Huybrechts et al. (1996); Payne et al. (2000); Bueler et al. (2005, 2007)
Iceberg	1	SSA	A&C	Jansen et al. (2005)
ISMIP-HOM	5 to 160	HOM	A	Pattyn (2003); Pattyn et al. (2008)
Full Stokes (lin. rheol.)	2	FS	A	Pattyn (2008)
Full Stokes (nonlin. rheol.)	2.5 to 10	FS	A	Thoma et al. (2010)
MISMIP	10	SIA/SSA	A	Pattyn et al. (2012)
MISMIP3d	5 to 20	SIA/SSA	A&C	Pattyn et al. (2013)
<i>Applications</i>				
<i>Subglacial Lake–Ice Sheet Interaction</i>				
Model coupling	2.5 to 10	FS	A	Thoma et al. (2010)
Vostok Subglacial Lake	5	FS	A	Thoma et al. (2012)
<i>Ice–Ocean Interaction</i>				
Model coupling	5	SIA/SSA	A	Determann et al. (2012)
Application to the FRIS domain	10	SIA/SSA	A	Determann et al. (2014)
<i>Earth System Modelling</i>				
Iterative coupling with COSMOS	20	SIA	A	Barbi et al. (2013)
Glacial Isostatic Adjustment	10 to 25	SIA/SSA	A	Konrad et al. (2013, 2014)
<i>Optional Modules</i>				
Balance water layer concept	5	SSA	A	Goeller et al. (2013a)
Tracer propagation	50	SIA	A	Sutter et al. (2013)

Table 2. Acronyms.

CISM	Community Ice Sheet Model
COSMOS	Community Earth System Models
FD	finite difference
FE	finite element
FS	full Stokes
FRIS	Filchner–Ronne Ice Shelf
gmres	generalised minimal residual
GRL	grounding line
GMT	generic mapping tools
HOM	higher order model
IPCC	Intergovernmental Panel on Climate Change
ISMIP-HOM	Ice Sheet Model Intercomparison Project for Higher-Order Models
ISSM	Ice Sheet System Model
LIS	Library of Iterative Solvers
MISMIP	Marine Ice Sheet Model Intercomparison Project
NR	Numerical Recipes
PenState3D	PennState3D ice-sheet/shelf model
PISM	Parallel Ice Sheet Model
RIMBAY	Revised Ice Model Based on frAnk pattYn
SIA	shallow ice approximation
SICOPOLIS	Simulation COde for POLythermal Ice Sheets
SSA	shallow shelf approximation
UMC	unstable manifold correction
VILMA	Viscoelastic Lithosphere and Mantle model
WAIS	West Antarctic Ice Sheet

the numerical model (with small effort) to new synthetic or realistic scenarios. Typical computational times needed by RIMBAY for some representative applications are given in Appendix C.

Based on the specific needs, RIMBAY can be applied easily to new scientific issues and is easy extensible because of well-structured interfaces. It provides a broad spectrum of applicability and functionality and could therefore contribute to solve the pressing questions of global climate change.

Appendix A

Ice evolution: continuity equation

The finite difference formulation of Eq. (37) for the ice thickness evolution is

$$\begin{aligned}
& \frac{H^{t+1} - H^t}{\Delta t} \\
& - f_{ad} \frac{D_{j+\frac{1}{2}}(H_{j+\frac{1}{2}}^{t+1} - H_j^{t+1}) - D_{j-\frac{1}{2}}(H_j^{t+1} - H_{j-1}^{t+1})}{(\Delta x)^2} \\
& - f_{ad} \frac{D_{i+\frac{1}{2}}(H_{i+\frac{1}{2}}^{t+1} - H_i^{t+1}) - D_{i-\frac{1}{2}}(H_i^{t+1} - H_{i-1}^{t+1})}{(\Delta y)^2} \\
& + (1 - f_{ad}) \frac{U_{j+\frac{1}{2}}H_{j+\frac{1}{2}}^{t+1} - U_{j-\frac{1}{2}}H_{j-\frac{1}{2}}^{t+1}}{\Delta x} \\
& + (1 - f_{ad}) \frac{V_{i+\frac{1}{2}}H_{i+\frac{1}{2}}^{t+1} - V_{i-\frac{1}{2}}H_{i-\frac{1}{2}}^{t+1}}{\Delta y} \\
& = f_{ad} \frac{D_{j+\frac{1}{2}}(B_{j+1} - B_j) - D_{j-\frac{1}{2}}(B_j - B_{j-1})}{(\Delta x)^2} \\
& + f_{ad} \frac{D_{i+\frac{1}{2}}(B_{i+1} - B_i) - D_{i-\frac{1}{2}}(B_i - B_{i-1})}{(\Delta y)^2} + \dot{m}, \quad (A1)
\end{aligned}$$

where the (diffusive) fluxes $D_{j+\frac{1}{2}} := (D_{j+1} + D_j)/2$ are defined on the edges (half way) between nodes. In Eq. (A1) subscripts i and j are omitted if they are constant in a specific term. The expanded form is

$$\begin{aligned}
& H^{t+1} \\
& - f_{ad} \frac{\Delta t}{2(\Delta x)^2} \left[(D_{j+1} + D_j)(H_{j+1}^{t+1} - H_j^{t+1}) \right. \\
& \quad \left. - (D_{j-1} + D_j)(H_j^{t+1} - H_{j-1}^{t+1}) \right] \\
& - f_{ad} \frac{\Delta t}{2(\Delta y)^2} \left[(D_{i+1} + D_i)(H_{i+1}^{t+1} - H_i^{t+1}) \right. \\
& \quad \left. - (D_{i-1} + D_i)(H_i^{t+1} - H_{i-1}^{t+1}) \right] \\
& + (1 - f_{ad}) \frac{\Delta t}{4\Delta x} \left[(U_{j+1} + u_j)(H_{j+1}^{t+1} + H_j^{t+1}) \right. \\
& \quad \left. - (U_{j-1} + u_j)(H_j^{t+1} + H_{j-1}^{t+1}) \right]
\end{aligned}$$

$$\begin{aligned}
& + (1 - f_{ad}) \frac{\Delta t}{4\Delta y} \left[(V_{i+1} + v_i)(H_{i+1}^{t+1} + H_i^{t+1}) \right. \\
& \quad \left. - (V_{i-1} + v_i)(H_i^{t+1} + H_{i-1}^{t+1}) \right] \\
& = f_{ad} \frac{\Delta t}{2(\Delta x)^2} \left[(D_{j+1} + D_j)(B_{j+1} - B_j) \right. \\
& \quad \left. - (D_{j-1} + D_j)(B_j - B_{j-1}) \right] \\
& + f_{ad} \frac{\Delta t}{2(\Delta y)^2} \left[(D_{i+1} + D_i)(B_{i+1} - B_i) \right. \\
& \quad \left. - (D_{i-1} + D_i)(B_i - B_{i-1}) \right] \\
& + (1 - f_{ad}) \frac{H_{j+1}^t + H_{j-1}^t + H_{i+1}^t + H_{i-1}^t}{4} \\
& + f_{ad} H^t + M \Delta t. \quad (A2)
\end{aligned}$$

The subscripts i and j which do not change within a specific term are omitted. The averaging of H^t on the right-hand side corresponds to a numerical *Lax scheme* diffusion and stabilises the otherwise unconditional unstable numerical scheme (e.g. Press et al., 2007). Sorting Eq. (A2) with respect to H_{ij}^{t+1} according to the node positions indicated in Fig. 4 and separation of the diffusive and advective parts according to

$$C_i = f_{ad} C_i^d + (1 - f_{ad}) C_i^a \quad (A3)$$

leads to the following coefficients:

$$\begin{aligned}
C_1^d &= -\frac{\Delta t}{2(\Delta y)^2} (D_i + D_{i-1}), \\
C_2^d &= -\frac{\Delta t}{2(\Delta x)^2} (D_j + D_{j-1}), \\
C_3^d &= 1 + \frac{\Delta t}{2} \left(\frac{2D_j + D_{j+1} + D_{j-1}}{(\Delta x)^2} + \frac{2D_i + D_{i+1} + D_{i-1}}{(\Delta y)^2} \right), \\
C_4^d &= -\frac{\Delta t}{2(\Delta x)^2} (D_j + D_{j+1}), \\
C_5^d &= -\frac{\Delta t}{2(\Delta y)^2} (D_i + D_{i+1}), \\
C_1^a &= -\frac{\Delta t}{4\Delta y} (V_i + V_{i-1}), \\
C_2^a &= -\frac{\Delta t}{4\Delta x} (U_j + U_{j-1}), \\
C_3^a &= 1 + \frac{\Delta t}{4} \left(\frac{U_{j+1} - U_{j-1}}{\Delta x} + \frac{V_{i+1} - V_{i-1}}{\Delta y} \right), \\
C_4^a &= +\frac{\Delta t}{4\Delta x} (U_j + U_{j+1}), \\
C_5^a &= +\frac{\Delta t}{4\Delta y} (V_i + V_{i+1}), \\
b_n &= f_{ad} \left[C_2^d (B_j - B_{j-1}) - C_4^d (B_{j+1} - B_j) \right. \\
& \quad \left. + C_1^d (B_i - B_{i-1}) - C_5^d (B_{i+1} - B_i) \right] \\
& + \frac{1 - f_{ad}}{4} (H_{j-1}^t + H_{j+1}^t + H_{i-1}^t + H_{i+1}^t) \\
& + f_{ad} H^t + \dot{m} \Delta t. \quad (A4)
\end{aligned}$$

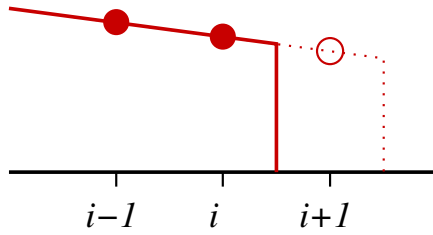


Fig. A1. Extrapolation of ice thickness H at open boundaries.

These coefficients represent the non-zero elements of a single row n for each i_j element of the matrix A_{nm} , while b_n represents the right-hand side of Eq. (A2).

Boundary conditions have to be formulated at the edges of the ice body. In case of open boundaries, the unknown value ψ_{i+1} is virtually extrapolated from the interior.

$$\psi_{i+1} = 2\psi_i - \psi_{i-1} \quad (\text{A5})$$

An example for the ice thickness H is illustrated in Fig. A1. Substitution of the ice thickness H , the velocity v_i , the diffusion D_i , and the ice bottom B on the eastern edge according to Eq. (A5) as well as on the southern edge according to $\psi_{j-1} = 2\psi_j - \psi_{j-1}$ in Eq. (A2) results in the highlighted modifications:

$$\begin{aligned} & H^{t+1} \\ & - f_{ad} \frac{\Delta t}{2(\Delta x)^2} 2(D_j - D_{j-1})(H_j^{t+1} - H_{j-1}^{t+1}) \\ & - f_{ad} \frac{\Delta t}{2(\Delta y)^2} 2(D_{i+1} - D_i)(H_{i+1}^{t+1} - H_i^{t+1}) \\ & + (1 - f_{ad}) \frac{\Delta t}{4\Delta x} \left[(3U_j - U_{j-1})(3H_j^{t+1} - H_{j-1}^{t+1}) \right. \\ & \quad \left. - (U_{j-1} + U_j)(H_j^{t+1} + H_{j-1}^{t+1}) \right] \\ & + (1 - f_{ad}) \frac{\Delta t}{4\Delta y} \left[(V_{i+1} + V_i)(H_{i+1}^{t+1} + H_i^{t+1}) \right. \\ & \quad \left. - (3V_i - V_{i+1})(3H_i^{t+1} - H_{i+1}^{t+1}) \right] \\ & = f_{ad} \frac{\Delta t}{2(\Delta x)^2} 2(D_j - D_{j-1})(B_j - B_{j-1}) \\ & = + f_{ad} \frac{\Delta t}{2(\Delta y)^2} 2(D_{i+1} - D_i)(B_{i+1} - B_i) \\ & + f_{ad} H^t + (1 - f_{ad}) \frac{0 + H_{j-1}^t + H_{i+1}^t + 0}{1 + 1} + \dot{m} \Delta t, \quad (\text{A6}) \end{aligned}$$

and consequently in

$$\begin{aligned} & C_1^d = 0, \\ & C_2^d = \frac{\Delta t}{2(\Delta x)^2} 2(D_j - D_{j-1}), \\ & C_3^d = 1 + \frac{\Delta t}{2} \left(\frac{2(D_{j-1} - D_j)}{(\Delta x)^2} + \frac{2(D_{i+1} - D_i)}{(\Delta y)^2} \right) \end{aligned}$$

$$\begin{aligned} & C_4^d = 0, \\ & C_5^d = \frac{\Delta t}{2(\Delta y)^2} 2(D_i - D_{i+1}), \\ & C_1^a = 0, \\ & C_2^a = -\frac{\Delta t}{4\Delta x} 4U_j, \\ & C_3^a = 1 + \frac{\Delta t}{4} \left(\frac{8U_j - 4U_{j-1}}{\Delta x} + \frac{4V_{i+1} - 8V_i}{\Delta y} \right), \\ & C_4^a = 0, \\ & C_5^a = +\frac{\Delta t}{4\Delta y} 4V_i, \\ & b_n = f_{ad} \left[C_2^d (B_j - B_{j-1}) - C_5^d (B_{i+1} - B_i) \right] \\ & \quad + \frac{1 - f_{ad}}{2} (H_{j-1}^t + H_{i+1}^t) \\ & \quad + f_{ad} H^t + \dot{m} \Delta t. \quad (\text{A7}) \end{aligned}$$

If the ice adjoins a nunatak, closed boundary conditions are applied. In this case the ice thickness H_{i+1} , the normal velocity $u_{i+\frac{1}{2}}$, and the diffusion $D_{i+\frac{1}{2}}$ vanish in Eq. (34). Alternatively we can express the unknown value ψ_{i+1} with

$$\begin{aligned} \psi_{i+\frac{1}{2}} &= \frac{\psi_i + \psi_{i+1}}{2} = 0 \quad \text{or} \\ \psi_{i+1} &= -\psi_i. \quad (\text{A8}) \end{aligned}$$

Substituting the ice thickness $H_{j+1} = 0$, the velocity $U_{j+1} = -U_j$, the diffusion $D_{j+1} = -D_j$, and the ice base $B_{j+1} = -B_j$ on the eastern edge as well as $H_{i-1} = -H_i$, $V_{i-1} = -V_i$, $D_{i-1} = -D_i$, and $B_{i-1} = -B_i$ on the southern edge results in the highlighted modifications with respect to Eq. (A2):

$$\begin{aligned} & H^{t+1} \\ & - f_{ad} \frac{\Delta t}{2(\Delta x)^2} \left[0 - (D_{j-1} + D_j)(H_j^{t+1} - H_{j-1}^{t+1}) \right] \\ & - f_{ad} \frac{\Delta t}{2(\Delta y)^2} \left[(D_i + D_{i+1})(H_{i+1}^{t+1} - H_i^{t+1}) - 0 \right] \\ & + (1 - f_{ad}) \frac{\Delta t}{4\Delta x} \left[0 - (U_{j-1} + U_j)(H_{j-1}^{t+1} + H_j^{t+1}) \right] \\ & + (1 - f_{ad}) \frac{\Delta t}{4\Delta y} \left[(V_i + V_{i+1})(H_i^{t+1} + H_{i+1}^{t+1}) - 0 \right] \\ & = f_{ad} \frac{\Delta t}{2(\Delta x)^2} \left[0 - (D_{j-1} + D_j)(B_j - B_{j-1}) \right] \\ & + f_{ad} \frac{\Delta t}{2(\Delta y)^2} \left[(D_i + D_{i+1})(B_{i+1} - B_i) - 0 \right] \\ & + f_{ad} H^t + (1 - f_{ad}) \frac{0 + H_{j-1}^t + H_{i+1}^t + 0}{1 + 1} + \dot{m} \Delta t, \quad (\text{A9}) \end{aligned}$$

and consequently in

$$C_1^d = 0,$$

$$\begin{aligned}
C_2^d &= -\frac{\Delta t}{2(\Delta x)^2} (D_{j-1} + D_j), \\
C_3^d &= 1 + \frac{\Delta t}{2} \left(\frac{D_{j-1} + D_j}{(\Delta x)^2} + \frac{D_i + D_{i+1}}{(\Delta y)^2} \right), \\
C_4^d &= 0, \\
C_5^d &= -\frac{\Delta t}{2(\Delta y)^2} (D_i + D_{i+1}), \\
C_1^a &= 0, \\
C_2^a &= -\frac{\Delta t}{4\Delta x} (U_{j-1} + U_j), \\
C_3^a &= 1 + \frac{\Delta t}{4} \left(-\frac{U_{j-1} + U_j}{\Delta x} + \frac{V_i + V_{i+1}}{\Delta y} \right), \\
C_4^a &= 0, \\
C_5^a &= +\frac{\Delta t}{4\Delta y} (V_i + V_{i+1}), \\
b_n &= f_{ad} \left[C_2^d (B_j - B_{j-1}) - C_5^d (B_{i+1} - B_i) \right] \\
&\quad + \frac{1 - f_{ad}}{2} (H_{j-1}^t + H_{i+1}^t) \\
&\quad + f_{ad} H^t + \dot{m} \Delta t.
\end{aligned} \tag{A10}$$

Appendix B

Velocity: shallow shelf approximation

Reformulating Eq. (16) and sorting with respect to the vertically averaged velocities U and V leads to

$$\begin{aligned}
&\frac{\partial}{\partial x} \left(4\mu H \frac{\partial U}{\partial x} \right) + \frac{\partial}{\partial y} \left(\mu H \frac{\partial U}{\partial y} \right) - \beta^2 U \\
&= \rho g H \frac{\partial S}{\partial x} - \frac{\partial}{\partial x} \left(2\mu H \frac{\partial V}{\partial y} \right) - \frac{\partial}{\partial y} \left(\mu H \frac{\partial V}{\partial x} \right), \\
&\frac{\partial}{\partial y} \left(4\mu H \frac{\partial V}{\partial y} \right) + \frac{\partial}{\partial x} \left(\mu H \frac{\partial V}{\partial x} \right) - \beta^2 V \\
&= \rho g H \frac{\partial S}{\partial y} - \frac{\partial}{\partial y} \left(2\mu H \frac{\partial U}{\partial x} \right) - \frac{\partial}{\partial x} \left(\mu H \frac{\partial U}{\partial y} \right).
\end{aligned} \tag{B1}$$

On the Arakawa C-grid (Fig. 3) the velocities are defined in-between the thickness (and viscosity) nodes. Defining the increments:

$$\Delta x_{i,j}^u := 0.5 \cdot (\Delta x_{i,j}^H + \Delta x_{i,j+1}^H), \tag{B2}$$

$$\Delta y_{i,j}^v := 0.5 \cdot (\Delta y_{i,j}^H + \Delta y_{i+1,j}^H), \tag{B3}$$

$$\Delta x_{i,j}^* := 0.5 \cdot (\Delta x_{i,j}^u + \Delta x_{i+1,j}^u), \tag{B4}$$

$$\Delta y_{i,j}^* := 0.5 \cdot (\Delta y_{i,j}^v + \Delta y_{i,j+1}^v), \tag{B5}$$

and $\xi := \mu H$ the finite difference version of Eq. (B1) is

$$\begin{aligned}
&\frac{4\xi_{i,j+1} \frac{U_{i,j+1} - U_{i,j}}{\Delta x_{i,j+1}^h} - 4\xi_{i,j} \frac{U_{i,j} - U_{i,j-1}}{\Delta x_{i,j}^h}}{\Delta x_{i,j}^u} \\
&+ \frac{\xi_{i+\frac{1}{2},j+\frac{1}{2}}^* \frac{U_{i+1,j} - U_{i,j}}{\Delta y_{i,j}^*} - \xi_{i-\frac{1}{2},j+\frac{1}{2}}^* \frac{U_{i,j} - U_{i-1,j}}{\Delta y_{i-1,j}^*}}{0.5(\Delta y_{i,j}^h + \Delta y_{i,j+1}^h)} \\
&- 0.5 \cdot (\beta_{i,j}^2 + \beta_{i,j+1}^2) U_{i,j} \\
&= \rho g \cdot 0.5 \cdot (H_{i,j} + H_{i,j+1}) \frac{S_{i,j+1} - S_{i,j}}{\Delta x_{i,j}^u} \\
&- \frac{2\xi_{i,j+1} \frac{V_{i,j+1} - V_{i-1,j+1}}{\Delta y_{i,j+1}^h} - 2\xi_{i,j} \frac{V_{i,j} - V_{i-1,j}}{\Delta y_{i,j}^h}}{\Delta x_{i,j}^u} \\
&- \frac{\xi_{i+\frac{1}{2},j+\frac{1}{2}}^* \frac{V_{i,j+1} - V_{i,j}}{\Delta x_{i,j}^*} - \xi_{i-\frac{1}{2},j+\frac{1}{2}}^* \frac{V_{i-1,j+1} - V_{i-1,j}}{\Delta x_{i-1,j}^*}}{0.5(\Delta y_{i,j}^h + \Delta y_{i,j+1}^h)},
\end{aligned} \tag{B6}$$

$$\begin{aligned}
&\frac{4\xi_{i+1,j} \frac{V_{i,j+1} - V_{i,j}}{\Delta y_{i+1,j}^h} - 4\xi_{i,j} \frac{V_{i,j} - V_{i,j-1}}{\Delta y_{i,j}^h}}{\Delta y_{i,j}^v} \\
&+ \frac{\xi_{i+\frac{1}{2},j+\frac{1}{2}}^* \frac{V_{i+1,j} - V_{i,j}}{\Delta x_{i,j}^*} - \xi_{i+\frac{1}{2},j-\frac{1}{2}}^* \frac{V_{i,j} - V_{i-1,j}}{\Delta x_{i,j-1}^*}}{0.5(\Delta x_{i,j}^h + \Delta x_{i+1,j}^h)} \\
&- 0.5 \cdot (\beta_{i,j}^2 + \beta_{i+1,j}^2) V_{i,j} \\
&= \rho g \cdot 0.5 \cdot (H_{i,j} + H_{i+1,j}) \frac{S_{i+1,j} - S_{i,j}}{\Delta y_{i,j}^v} \\
&- \frac{2\xi_{i+1,j} \frac{U_{i+1,j} - U_{i+1,j-1}}{\Delta x_{i+1,j}^h} - 2\xi_{i,j} \frac{U_{i,j} - U_{i,j-1}}{\Delta x_{i,j}^h}}{\Delta y_{i,j}^v} \\
&- \frac{\xi_{i+\frac{1}{2},j+\frac{1}{2}}^* \frac{U_{i+1,j} - U_{i,j}}{\Delta y_{i,j}^*} - \xi_{i+\frac{1}{2},j-\frac{1}{2}}^* \frac{U_{i+1,j-1} - U_{i,j-1}}{\Delta y_{i,j-1}^*}}{0.5(\Delta x_{i,j}^h + \Delta x_{i+1,j}^h)},
\end{aligned} \tag{B7}$$

with

$$\xi_{i+\frac{1}{2},j+\frac{1}{2}}^* := \frac{1}{4} (\xi_{i,j} + \xi_{i,j+1} + \xi_{i+1,j} + \xi_{i+1,j+1}),$$

$$\xi_{i-\frac{1}{2},j+\frac{1}{2}}^* := \frac{1}{4} (\xi_{i,j} + \xi_{i,j+1} + \xi_{i-1,j} + \xi_{i-1,j+1}),$$

$$\xi_{i+\frac{1}{2},j-\frac{1}{2}}^* := \frac{1}{4} (\xi_{i,j} + \xi_{i,j-1} + \xi_{i+1,j} + \xi_{i+1,j-1}).$$

Defining

$$\alpha_1^u := \frac{\xi_{i,j+1}}{\Delta x_{i,j}^u} \quad \gamma_1^u := \frac{2\xi_{i+\frac{1}{2},j+\frac{1}{2}}^*}{\Delta y_{i,j}^H + \Delta y_{i,j+1}^H},$$

$$\alpha_1^v := \frac{\xi_{i+1,j}}{\Delta y_{i,j}^v} \quad \gamma_1^v := \frac{2\xi_{i+\frac{1}{2},j+\frac{1}{2}}^*}{\Delta x_{i,j}^H + \Delta x_{i+1,j}^H},$$

$$\alpha_2^u := \frac{\xi_{i,j}}{\Delta x_{i,j}^u} \quad \gamma_2^u := \frac{2\xi_{i-\frac{1}{2},j+\frac{1}{2}}^*}{\Delta y_{i,j}^H + \Delta y_{i,j+1}^H},$$

$$\alpha_2^v := \frac{\xi_{i,j}}{\Delta y_{i,j}^v} \quad \gamma_2^v := \frac{2\xi_{i+\frac{1}{2},j-\frac{1}{2}}^*}{\Delta x_{i,j}^H + \Delta x_{i+1,j}^H},$$

the coefficients according to Fig. B1 and the forcing term (on the right-hand side) are given by

$$\begin{aligned} C_3^u &= \frac{\gamma_2^u}{\Delta y_{i-1,j}^*}, \\ C_4^u &= \frac{4\alpha_2^u}{\Delta x_{i,j}^H}, \\ C_5^u &= -\frac{4\alpha_1^u}{\Delta x_{i,j+1}^H} - \frac{4\alpha_2^u}{\Delta x_{i,j}^H} - \frac{\gamma_1^u}{\Delta y_{i,j}^*} - \frac{\gamma_2^u}{\Delta y_{i-1,j}^*} \\ &\quad - 0.5 \cdot (\beta_{i,j}^2 + \beta_{i,j+1}^2), \\ C_6^u &= \frac{4\alpha_1^u}{\Delta x_{i,j+1}^H}, \\ C_7^u &= \frac{\gamma_1^u}{\Delta y_{i,j}^*}, \\ b_m^u &= \rho g \cdot 0.5 \cdot (H_{i,j} + H_{i,j+1}) \frac{S_{i,j+1} - S_{i,j}}{\Delta x_{i,j}^u} \\ &\quad - \frac{2\alpha_1^u}{\Delta y_{i,j+1}^H} (V_{i,j+1} - V_{i-1,j+1}) \\ &\quad + \frac{2\alpha_2^u}{\Delta y_{i,j}^H} (V_{i,j} - V_{i-1,j}) \\ &\quad - \frac{\gamma_1^u}{\Delta x_{i,j}^*} (V_{i,j+1} - V_{i,j}) \\ &\quad + \frac{\gamma_2^u}{\Delta x_{i-1,j}^*} (V_{i-1,j+1} - V_{i-1,j}). \end{aligned} \quad (\text{B8})$$

$$\begin{aligned} C_3^v &= \frac{4\alpha_2^v}{\Delta y_{i,j}^H}, \\ C_4^v &= \frac{\gamma_2^v}{\Delta x_{i,j-1}^*}, \\ C_5^v &= -\frac{4\alpha_1^v}{\Delta y_{i+1,j}^H} - \frac{4\alpha_2^v}{\Delta y_{i,j}^H} - \frac{\gamma_1^v}{\Delta x_{i,j}^*} - \frac{\gamma_2^v}{\Delta x_{i,j-1}^*}, \\ &\quad - 0.5 \cdot (\beta_{i,j}^2 + \beta_{i+1,j}^2) \\ C_6^v &= \frac{\gamma_1^v}{\Delta x_{i,j}^*}, \\ C_7^v &= \frac{4\alpha_1^v}{\Delta y_{i+1,j}^H}, \\ b_n^v &= \rho g \cdot 0.5 \cdot (H_{i,j} + H_{i+1,j}) \frac{S_{i+1,j} - S_{i,j}}{\Delta y_{i,j}^v} \\ &\quad - \frac{2\alpha_1^v}{\Delta x_{i+1,j}^H} (U_{i+1,j} - U_{i+1,j-1}) \end{aligned}$$

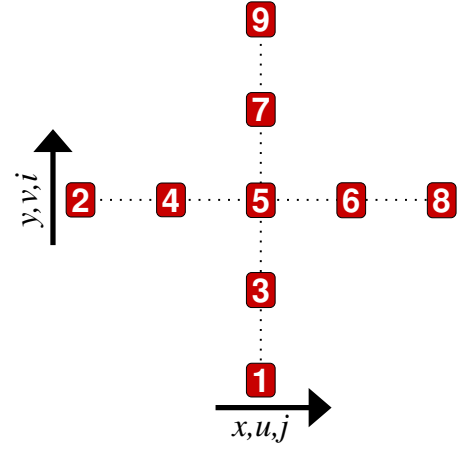


Fig. B1. Relative positions and numbering of nodes for the SSA.

$$\begin{aligned} &+ \frac{2\alpha_2^v}{\Delta x_{i,j}^H} (U_{i,j} - U_{i,j-1}) \\ &- \frac{\gamma_1^v}{\Delta x_{i,j}^*} (U_{i+1,j} - U_{i,j}) \\ &+ \frac{\gamma_2^v}{\Delta x_{i,j-1}^*} (U_{i+1,j-1} - U_{i,j-1}). \end{aligned} \quad (\text{B9})$$

The lateral boundary condition along the ice shelf front is defined as *free slip*, and hence

$$\frac{\partial U}{\partial y} = 0 \quad \frac{\partial V}{\partial x} = 0, \quad (\text{B10})$$

or

$$\begin{aligned} \text{N: } U_{i+1,j} &= U_{i,j} &\Rightarrow \gamma_1^u &= 0 \text{ in } C_7^u \text{ and } C_5^u, \\ \text{S: } U_{i-1,j} &= U_{i,j} &\Rightarrow \gamma_2^u &= 0 \text{ in } C_3^u \text{ and } C_5^u, \\ \text{E: } V_{i,j+1} &= V_{i,j} &\Rightarrow \gamma_1^v &= 0 \text{ in } C_6^v \text{ and } C_5^v, \\ \text{W: } V_{i,j-1} &= V_{i,j} &\Rightarrow \gamma_2^v &= 0 \text{ in } C_4^v \text{ and } C_5^v. \end{aligned}$$

In case of *no slip* boundary conditions, the flow on the boundary is zero, and hence

$$\frac{u_{i+1,j} + u_{i,j}}{2} = 0 \quad \frac{v_{i+1,j} + v_{i,j}}{2} = 0 \quad (\text{B11})$$

or

$$\begin{aligned} \text{N: } u_{i+1,j} &= -u_{i,j} &\Rightarrow \gamma_1^u &= 0 \text{ in } C_7^u \text{ and } 2 \text{ in } C_5^u, \\ \text{S: } u_{i-1,j} &= -u_{i,j} &\Rightarrow \gamma_2^u &= 0 \text{ in } C_3^u \text{ and } 2 \text{ in } C_5^u, \\ \text{E: } v_{i,j+1} &= -v_{i,j} &\Rightarrow \gamma_1^v &= 0 \text{ in } C_6^v \text{ and } 2 \text{ in } C_5^v, \\ \text{W: } v_{i,j-1} &= -v_{i,j} &\Rightarrow \gamma_2^v &= 0 \text{ in } C_4^v \text{ and } 2 \text{ in } C_5^v. \end{aligned}$$

Appendix C

Typical CPU wall-clock times

Typical CPU times needed by RIMBAY for some representative applications are given in Table C1.

Table C1. Typical CPU wall-clock times consumed to simulate typical domains with the specified numerical complexities.

Domain	Numerics	Resolution (km)	Integration time (yr)	CPU time (order)	Reference
Continental wide					
Antarctica	SIA	40	10^6	1 h	Sutter et al. (2013)
		20		1 day	Sutter et al. (2013)
Greenland	SIA/SSA	40	10^7	2 days	Sutter et al. (2013)
	SIA	20		2 h	P. Gierz (personal communication, 2013)
Regional					
WAIS	SIA/SSA	20	10^4	12 h	H. Konrad (personal communication, 2013)
Lake Vostok	SIA/FS*	10	10^3	1 h	Thoma et al. (2012)
Lake Vostok	SIA/FS*	5	10^6	5 days	Thoma et al. (2012)
FRIS	SIA/SSA	10	10^3	1 h	Determann et al. (2014)
Siple Coast	SSA	10	10^2	10 min	S. Goeller (personal communication, 2013)
Synthetic					
Eismint	SIA	25	10^7	1 h	Konrad et al. (2013)
Synthetic Bay	SIA/SSA	10	10^3	5 min	Konrad et al. (2014)
Iceberg	SSA	1	10^0	10 s	Fig. 6
		2	10^0	10 min	Fig. 7
ISMIP-HOM	HOM	4	10^2	2 min	re-calculating the 160 km experiment from Pattyn (2003)
ISMIP-HOM	HOM	1	10^2	30 min	re-calculating the 160 km experiment from Pattyn (2003)
Mismip	SIA/SSA	5	10^4	3 h	Pattyn et al. (2012)

*: about 30 percent of the whole domain (the lake and its vicinity) is calculated with a FS solver, note that there is no ice evolution in this experiment, only the ice temperature evolves over time.

Acknowledgements. This work was partly funded by the DFG through grant MA3347/2-1; it was supported by funding from the ice2sea program from the European Union 7th Framework Programme, grant number 226375; and from the Helmholtz Climate Initiative REKLIM (Regional Climate Change), a joint research project of the Helmholtz Association of German research centres (HGF), which is gratefully acknowledged. The authors wish to thank Sergey Danilov, Angelika Humbert, Thomas Kleiner, Hannes Konrad, Martin Losch, Silvia Massmann, and Johannes Sutter for fruitful discussions, Stephen Cornford, Helene Seroussi, Thomas Zwinger and an anonymous reviewer for their helpful suggestions which improved the manuscript.

Edited by: C. Ritz

References

- Arakawa, A. and Lamb, V. R.: Methods of computational physics, Vol. 17, Academic Press, 1977.
- Barbi, D., Lohmann, G., Grosfeld, K., and Thoma, M.: Ice sheet dynamics within an Earth system model: coupling and first results on ice stability and ocean circulation, *Geosci. Model Dev. Discuss.*, 6, 1–35, doi:10.5194/gmdd-6-1-2013, 2013.
- Bindschadler, R. A., Nowicki, S., Abe-Ouchi, A., Aschwanden, A., Choi, H., Fastook, J., Granzow, G., Greve, R., Gutowski, G., Herzfeld, U., Jackson, C., Johnson, J., Khroulev, C., Levermann, A., Lipscomb, W. H., Martin, M. A., Morlighem, M., Parizek, B. R., Pollard, D., Price, S. F., Ren, D., Saito, F., Sato, T., Seddik, H., Seroussi, H., Takahashi, K., Walker, R., and Wang, W. L.: Ice-sheet model sensitivities to environmental forcing and their use in projecting future sea level (the SeaRISE project), *J. Glaciol.*, 59, 195–224, doi:10.3189/2013JG12J125, 2013.
- Bougamont, M., Price, S., Christoffersen, P., and Payne, A. J.: Dynamic patterns of ice stream flow in a 3-D higher-order ice sheet model with plastic bed and simplified hydrology, *J. Geophys. Res.*, 116, 1–13, doi:10.1029/2011JF002025, 2011.
- Bueler, E., Lingle, C. S., Kallen-Brown, J. A., Covey, D. N., and Bowman, L. N.: Exact solutions and verification of numerical models for isothermal ice sheets, *J. Glaciol.*, 51, 291–306, doi:10.3189/172756505781829449, 2005.
- Bueler, E., Brown, J., and Lingle, C.: Exact solutions to the thermomechanically coupled shallow-ice approximation: effective tools for verification, *J. Glaciol.*, 53, 499–516, doi:10.3189/002214307783258396, 2007.
- Church, J. A., Gregory, J. M., White, N. J., Platten, S. M., and Mitrovica, J. X.: Understanding and projecting sea level change, *Oceanography*, 24, 130–143, doi:10.5670/oceanog.2011.33, 2011.
- Cornford, S. L., Martin, D. F., Graves, D. T., Ranken, D. F., Le Brocq, A. M., Gladstone, R. M., Payne, A. J., Ng, E. G., and Lipscomb, W. H.: Adaptive mesh, finite volume modeling of marine ice sheets, *J. Comp. Phys.*, 232, 529–549, doi:10.1016/j.jcp.2012.08.037, 2013.
- Cuffey, K. M. and Paterson, W. S. B.: *The Physics of Glaciers*, Elsevier, Oxford, 4th Edn., 2010.
- Determann, J., Thoma, M., Grosfeld, K., and Massmann, S.: Impact of ice shelf basal melting on inland ice-sheet thickness: A model study, *Ann. Glaciol.*, 53, 129–135, doi:10.3189/2012AoG60A170, 2012.

- Determann, J., Thoma, M., Grosfeld, K., and Hellmer, H.: Ocean warming beneath major Antarctic ice shelf raises century-scale sea-level projections, *Nature Climate Change*, in review, 2014.
- Docquier, D., Perichon, L., and Pattyn, F.: Representing grounding line dynamics in numerical ice sheet models: recent advances and outlook, *Surv. Geophys.*, 32, 417–435, doi:10.1007/s10712-011-9133-3, 2011.
- Drouet, A. S., Docquier, D., Durand, G., Hindmarsh, R., Pattyn, F., Gagliardini, O., and Zwinger, T.: Grounding line transient response in marine ice sheet models, *The Cryosphere*, 7, 395–406, doi:10.5194/tc-7-395-2013, 2013.
- Gillet-Chaulet, F., Gagliardini, O., Seddik, H., Nodet, M., Durand, G., Ritz, C., Zwinger, T., Greve, R., and Vaughan, D. G.: Greenland ice sheet contribution to sea-level rise from a new-generation ice-sheet model, *The Cryosphere*, 6, 1561–1576, doi:10.5194/tc-6-1561-2012, 2012.
- Gladstone, R. M., Lee, V., Vieli, A., and Payne, A. J.: Grounding line migration in an adaptive mesh ice sheet model, *J. Geophys. Res.*, 115, F04014, doi:10.1029/2009JF001615, 2010.
- Goeller, S., Thoma, M., Grosfeld, K., and Miller, H.: A balanced water layer concept for subglacial hydrology in large-scale ice sheet models, *The Cryosphere*, 7, 1095–1106, doi:10.5194/tc-7-1095-2013, 2013a.
- Greve, R.: Thermomechanisches Verhalten polythermer Eisschilde – Theorie, Analytik, Numerik, Berichte aus der Geowissenschaft, Shaker Verlag, doctoral thesis, Department of Mechanics, Darmstadt University of Technology, Germany, ISBN: 3-8265-0999-4, 1995.
- Greve, R. and Blatter, H.: *Dynamics of Ice Sheets and Glaciers, Advances in Geophysical and Environmental Mechanics and Mathematics*, Springer, 2009.
- Hanson, S., Nicholls, R., Ranger, N., Hallegatte, S., Corfee-Morlot, J., Herweijer, C., and Chateau, J.: A global ranking of port cities with high exposure to climate extremes, *Climatic Change*, 104, 89–111, doi:10.1007/s10584-010-9977-4, 2011.
- Hindmarsh, R. C. A. and Payne, A. J.: Time-step limits for stable solutions of the ice-sheet equation, *Ann. Glaciol.*, 23, 74–85, 1996.
- Hooke, R. L.: Flow law for polycrystalline ice in glaciers: Comparison of theoretical predictions, laboratory data, and field measurements, *Rev. Geophys. Space Phys.*, 19, 664–672, 1981.
- Hutter, K.: *Theoretical glaciology: material science of ice and the mechanics of glaciers and ice sheets*, D. Reidel Publishing Company, Terra Scientific Publishing Company, ISBN 90-277-1473-8, 1983.
- Huybrechts, P., Payne, T., Ouchi, A. A. O., Calov, R., A., F., Fastook, J. L., Greve, R., Hindmarsh, R. C. A., Hoydal, O., and Jóhannesson, T.: The EISMINT benchmarks for testing ice-sheet models, *Ann. Glaciol.*, 23, 1–12, 1996.
- IPCC: *The Physical Science Basis, Contribution of Working Group I to the Fourth Assessment Report of the Intergovernmental Panel on Climate Change*, in: *Climate Change 2007*, edited by: Solomon, S., Qin, D., Manning, M., Chen, Z., Marquis, M., Averyt, K. B., Tignor, M., and Miller, H. L., Cambridge University Press, Cambridge, United Kingdom and New York, NY, USA, 2007.
- Jansen, D., Sandhäger, H., and Rack, W.: Model experiments on large tabular iceberg evolution: ablation and strain thinning, *J. Glaciol.*, 51, 363–372, doi:10.3189/172756505781829313, 2005.
- Joughin, I., Tulaczyk, S., Bamber, J. L., Blankenship, D., Holt, J. W., Scambos, T., and Vaughan, D. G.: Basal conditions for Pine Island and Thwaites Glaciers, West Antarctica, determined using satellite and airborne data, *J. Glaciol.*, 55, 245–257, doi:10.3189/002214309788608705, 2009.
- Konrad, H., Thoma, M., Sasgen, I., Klemann, V., Grosfeld, K., Barbi, D., and Martinec, Z.: The Deformational Response of a Viscoelastic Solid Earth Model Coupled to a Thermo-mechanical Ice Sheet Model, *Surv. Geophys.*, online first, doi:10.1007/s10712-013-9257-8, 2013.
- Konrad, H., Sasgen, I., Klemann, V., Thoma, M., Grosfeld, K., and Martinec, Z.: Sensitivity of grounding line dynamics to viscoelastic deformation of the solid Earth, *J. Geophys. Res.*, submitted, 2014.
- Larour, E., Seroussi, H., Morlighem, M., and Rignot, E.: Continental scale, high order, high spatial resolution, ice sheet modeling using the Ice Sheet System Model (ISSM), *J. Geophys. Res.*, 117, 1–20, doi:10.1029/2011JF002140, 2012.
- Lemieux, J.-F., Price, S. F., Evans, K. J., Knoll, D., Salinger, A. G., Holland, D. M., and Payne, A. J.: Implementation of the Jacobian-free Newton–Krylov method for solving the first-order ice sheet momentum balance, *J. Comp. Phys.*, 230, 6531–6545, doi:10.1016/j.jcp.2011.04.037, 2011.
- Levermann, A., Winkelmann, R., Nowicki, S., Fastook, J. L., Frieler, K., Greve, R., Hellmer, H. H., Martin, M. A., Mengel, M., Payne, A. J., Pollard, D., Sato, T., Timmermann, R., Wang, W. L., and Bindshadler, R. A.: Projecting Antarctic ice discharge using response functions from SeaRISE ice-sheet models, *The Cryosphere Discuss.*, 6, 3447–3489, doi:10.5194/tcd-6-3447-2012, 2012.
- MacAyeal, D. R.: Large-scale ice flow over a viscous basal sediment: Theory and application to Ice Stream B, Antarctica, *J. Geophys. Res.*, 94, 4071–4087, doi:10.1029/JB094iB04p04071, 1989.
- Martin, M. A., Winkelmann, R., Haseloff, M., Albrecht, T., Bueler, E., Khroulev, C., and Levermann, A.: The Potsdam Parallel Ice Sheet Model (PISM-PIK) – Part 2: Dynamic equilibrium simulation of the Antarctic ice sheet, *The Cryosphere*, 5, 727–740, doi:10.5194/tc-5-727-2011, 2011.
- Morland, L.: Unconfined Ice-Shelf Flow, in: *Dynamics of the West Antarctic Ice Sheet*, edited by: Veen, C. J. and Oerlemans, J., Vol. 4, *Glaciology and Quaternary Geology*, 99–116, Springer Netherlands, doi:10.1007/978-94-009-3745-1_6, 1987.
- Nishida, A.: Experience in developing an open source scalable software infrastructure in Japan, in: *Computational science and its applications – ICCSA*, edited by: Taniar, D., Gervasi, O., Murgante, B., Pardede, E., and Apduhan, B. O., Vol. 6017, *Lecture Notes in Computer Science*, 448–462, Springer, doi:10.1007/978-3-642-12165-4_36, 2010.
- Paterson, W. S. B.: *The Physics of Glaciers*, Butterworth Heinemann, Oxford, 3rd Edn., 1994.
- Paterson, W. S. B. and Budd, W. F.: Flow parameters for ice sheet modeling, *Cold Reg. Sci. Technol.*, 6, 175–177, doi:10.1016/0165-232X(82)90010-6, 1982.
- Pattyn, F.: Ice-sheet modelling at different spatial resolutions: focus on the grounding zone, *Ann. Glaciol.*, 31, 211–216, doi:10.3189/172756400781820435, 2000.

- Pattyn, F.: Transient glacier response with a higher-order numerical ice-flow model, *J. Glaciol.*, 48, 467–477, doi:10.3189/172756502781831278, 2002.
- Pattyn, F.: A new three-dimensional higher-order thermomechanical ice sheet model: Basic sensitivity, ice stream development, and ice flow across subglacial lakes, *J. Geophys. Res.*, 108, 1–15, doi:10.1029/2002JB002329, 2003.
- Pattyn, F.: Investigating the stability of subglacial lakes with a full Stokes ice-sheet model, *J. Glaciol.*, 54, 353–361, doi:10.3189/002214308784886171, 2008.
- Pattyn, F.: Antarctic subglacial conditions inferred from a hybrid ice sheet/ice stream model, *Earth Planet. Sc. Lett.*, 295, 451–461, doi:10.1016/j.epsl.2010.04.025, 2010.
- Pattyn, F., de Smedt, B., and Souchez, R.: Influence of subglacial Vostok lake on the regional ice dynamics of the Antarctic ice sheet: a model study, *J. Glaciol.*, 50, 583–589, 2004.
- Pattyn, F., Huyghe, A., De Brabander, S., and De Smedt, B.: Role of transition zones in marine ice sheet dynamics, *J. Geophys. Res.*, 111, F02004, 1–10, doi:10.1029/2005JF000394, 2006.
- Pattyn, F., Perichon, L., Aschwanden, A., Breuer, B., de Smedt, B., Gagliardini, O., Gudmundsson, G. H., Hindmarsh, R. C. A., Hubbard, A., Johnson, J. V., Kleiner, T., Kononov, Y., Martin, C., Payne, A. J., Pollard, D., Price, S., Rückamp, M., Saito, F., Souček, O., Sugiyama, S., and Zwinger, T.: Benchmark experiments for higher-order and full-Stokes ice sheet models (ISMIP-HOM), *The Cryosphere*, 2, 95–108, doi:10.5194/tc-2-95-2008, 2008.
- Pattyn, F., Schoof, C., Perichon, L., Hindmarsh, R. C. A., Bueler, E., de Fleurian, B., Durand, G., Gagliardini, O., Gladstone, R., Goldberg, D., Gudmundsson, G. H., Huybrechts, P., Lee, V., Nick, F. M., Payne, A. J., Pollard, D., Rybak, O., Saito, F., and Vieli, A.: Results of the Marine Ice Sheet Model Intercomparison Project, MISIP, *The Cryosphere*, 6, 573–588, doi:10.5194/tc-6-573-2012, 2012.
- Pattyn, F., Perichon, L., Durand, G., Favier, L., Gagliardini, O., Hindmarsh, R. C. A., Zwinger, T., Albrecht, T., Cornford, S., Docquier, D., Fürst, J. J., Goldberg, D., Gudmundsson, G. H., Humbert, A., Hutten, M., Huybrechts, P., Jouvét, G., Kleiner, T., Larour, E., Martin, D., Morlighem, M., Payne, A. J., Pollard, D., Rückamp, M., Rybak, O., Seroussi, H., Thoma, M., and Wilkens, N.: Grounding-line migration in plan-view marine ice-sheet models: results of the *ice2sea* MISIP3d intercomparison, *J. Glaciol.*, 59, 410–422, doi:10.3189/2013JoG12J129, 2013.
- Payne, A. J.: A thermomechanical model of ice flow in West Antarctica, *Clim. Dynam.*, 15, 115–125, doi:10.1007/s003820050271, 1999.
- Payne, A. J., Huybrechts, P., Abe-Ouchi, A., Calov, R., Fastook, J. L., Greve, R., Marshall, S. J., Marsiat, I., Ritz, C., Tarasov, L., and Thomassen, M. P. A.: Results from the EISMINT model intercomparison: the effects of thermomechanical coupling, *J. Glaciol.*, 46, 227–238, doi:10.3189/172756500781832891, 2000.
- Pollard, D. and DeConto, R. M.: Modelling West Antarctic ice sheet growth and collapse through the past five million years, *Nature*, 458, 329–332, doi:10.1038/nature07809, 2009.
- Pollard, D. and DeConto, R. M.: Description of a hybrid ice sheet-shelf model, and application to Antarctica, *Geosci. Model Dev.*, 5, 1273–1295, doi:10.5194/gmd-5-1273-2012, 2012.
- Press, W. H., Teukolsky, S. A., Vetterling, W. T., and Flannery, B. P.: *Numerical Recipes 3rd Edn., The Art of Scientific Computing*, Cambridge University Press, New York, NY, USA, 3 Edn., 2007.
- Purser, R. J. and Leslie, L. M.: A semi-implicit, semi-Lagrangian finite-difference scheme using high-order spatial differencing on a nonstaggered grid, *Mon. Weather Rev.*, 116, 2069–2080, 1988.
- Rahmstorf, S., Foster, G., and Cazenave, A.: Comparing climate projections to observations up to 2011, *Environ. Res. Lett.*, 7, 044035, doi:10.1088/1748-9326/7/4/044035, 2012.
- Rutt, I. C., Hagdorn, M., Hulton, N. R. J., and Payne, A. J.: The Glimmer community ice sheet model, *J. Geophys. Res.*, 114, 1–22, doi:10.1029/2008JF001015, 2009.
- Sandhäger, H.: *Quantifizierung eisdynamischer und massenhaushaltsrelevanter Basisgrößen eines antarktischen Inland-Schelfeis-Systems unter Einsatz eines numerischen Fließmodells*, Ph.D. thesis, Westfälische Wilhelms-Universität Münster, 2000.
- Sato, T. and Greve, R.: Sensitivity experiments for the Antarctic ice sheet with varied sub-ice-shelf melting rates, *Ann. Glaciol.*, 53, 221–228, doi:10.3189/2012AoG60A042, 2012.
- Schoof, C.: Ice sheet grounding line dynamics: Steady states, stability, and hysteresis, *J. Geophys. Res.*, 112, 1–19, doi:10.1029/2006JF000664, 2007.
- Seroussi, H., Ben Dhia, H., Morlighem, M., Larour, E., Rignot, E., and Aubry, D.: Coupling ice flow models of varying orders of complexity with the Tiling method, *J. Glaciol.*, 58, 776–786, doi:10.3189/2012JoG11J195, 2012.
- Sutter, J., Lohmann, G., Thoma, M., Barbi, D., and Werner, M.: 3D tracer advection in polar ice sheets: modeling stratigraphy and isotope distributions in Greenland & Antarctica, Poster, *Geophys. Res. Abstr.*, EGU2013-10731, EGU General Assembly 2013, Vienna, Austria, 2013.
- Thoma, M., Grosfeld, K., Mayer, C., and Pattyn, F.: Interaction between ice sheet dynamics and subglacial lake circulation: a coupled modelling approach, *The Cryosphere*, 4, 1–12, doi:10.5194/tc-4-1-2010, 2010.
- Thoma, M., Grosfeld, K., Mayer, C., and Pattyn, F.: Ice flow sensitivity to boundary processes: A coupled model study in the Vostok Subglacial Lake area, *Ann. Glaciol.*, 53, 173–180, doi:10.3189/2012AoG60A009, 2012.
- Van der Veen, C. J. and Whillans, I. M.: Force budget: I. Theory and numerical methods, *J. Glaciol.*, 35, 53–60, doi:10.3189/002214389793701581, 1989.
- Wessel, P. and Smith, W. H. F.: New, improved version of Generic Mapping Tools released, *EOS T. Am. Geophys. Un.*, 79, 579–579, doi:10.1029/98EO00426, 1998.
- Wessel, P., Smith, W. H. F., Scharroo, R., Luis, J. F., and Wobbe, F.: *Generic Mapping Tools: Improved Version Released*, *EOS T. Am. Geophys. Un.*, 94, 409–410, doi:10.1002/2013EO450001, 2013.
- Winkelmann, R., Martin, M. A., Haseloff, M., Albrecht, T., Bueler, E., Khroulev, C., and Levermann, A.: The Potsdam Parallel Ice Sheet Model (PISM-PIK) – Part 1: Model description, *The Cryosphere*, 5, 715–726, doi:10.5194/tc-5-715-2011, 2011.
- Zwinger, T., Greve, R., Gagliardini, O., Shiraiwa, T., and Lyly, M.: A full Stokes-flow thermo-mechanical model for firn and ice applied to the Gorshkov crater glacier, Kamchatka, *Ann. Glaciol.*, 45, 29–37, doi:10.3189/172756407782282543, 2007.